The Chemical Sensitivity of Stratospheric Ozone to N_2O and CH_4 through the 21st Century

A thesis submitted in partial fulfilment of the requirements

for the Degree of Doctor of Philosophy in Chemistry

in the University of Canterbury by

Laura E. Revell

University of Canterbury

2012

Abstract

Through the 21st century, global-mean stratospheric ozone abundances are projected to increase due to decreasing chlorine and bromine concentrations (as a consequence of the Montreal Protocol), and continued CO_2-induced cooling of the stratosphere. Along with CO_2, anthropogenic emissions of the greenhouse gases N_2O and CH_4 are projected to increase, thus increasing their atmospheric concentrations. Consequently, reactive nitrogen species (NO_x) produced from N_2O and reactive hydrogen species (HO_x) produced from CH_4 are expected to play an increasingly important role in determining stratospheric ozone concentrations. In this thesis chemistry-climate model (CCM) simulations were performed using the NIWA-SOCOL CCM, which tracks the contributions to ozone loss from a prescribed set of catalytic cycles, including the ozone-depleting NO_x and HO_x cycles, over latitude, longitude, pressure and time.

It was recently shown that, of the ozone-depleting substances currently being emitted, N_2O emissions dominate, and are likely to do so throughout the 21st century. To investigate the links between N_2O and NO_x concentrations, and the effects of NO_x on stratospheric ozone in a changing climate, a CCM simulation of the evolution of ozone from 1960 to 2100 was performed, using the IPCC SRES A1B scenario for greenhouse gases. It was found that the yield of NO_x from N_2O is reduced due to stratospheric cooling and a strengthening of the Brewer-Dobson circulation. After accounting for the reduced NO_x yield, additional weakening of the primary ozone-depleting NO_x cycle is attributed to reduced availability of atomic oxygen, due to a) stratospheric cooling decreasing the atomic oxygen/ozone ratio, and b) enhanced rates of chlorine-catalysed ozone-loss cycles around the year 2000 and enhanced rates of HO_x-induced ozone depletion through the 21st century. These results suggest that the effects of N_2O on ozone depend on both the radiative and chemical environment of the upper stratosphere; specifically CO_2-induced cooling of the stratosphere and elevated CH_4 emissions, which enhance HO_x-induced ozone loss and reduce the availability of atomic oxygen to participate in NO_x ozone-loss cycles.

Because CO_2-induced stratospheric cooling reduces the effectiveness of N_2O in depleting stratospheric ozone, it follows that a scenario in which emissions of N_2O undergo a larger increase through the 21st century, while emissions of CO_2 undergo a smaller increase than they do in the SRES A1B scenario, could be damaging to stratospheric ozone. Such a scenario could occur if biofuels production and consumption became widespread; biofuels are becoming increasingly popular sources of renewable energy as economic pressures and environmental consequences

encourage the use of alternatives to fossil fuels. Growing crops destined for use as biofuels incurs large N_2O emissions associated with the use of nitrogen-based fertilizers and, because biofuels are carbon-neutral, future increases in CO_2 would likely be smaller than they are in the SRES A1B scenario.

The potential effects on the ozone layer of a large-scale shift away from fossil fuel use to biofuels consumption over the 21st century were examined. Under such a scenario, global-mean column ozone decreases by 2.6 DU between 2010 and 2100 in contrast to a 0.7 DU decrease under a SRES B1 control simulation and a 9.1 DU increase under the SRES A1B scenario. Two factors cause the decrease in ozone in the biofuels simulation: 1) large N_2O emissions lead to faster rates of the ozone-depleting NO_x cycles and; 2) reduced CO_2 emissions (due to reduced fossil fuel burning) lead to relatively less stratospheric cooling over the 21st century, which decreases ozone abundances. Reducing CO_2 emissions while neglecting to reduce N_2O emissions could therefore be damaging to the ozone layer.

To assess the sensitivity of stratospheric ozone to different emissions scenarios for N_2O and CH_4, eight CCM simulations were performed for the period 2015-2100. In all of these simulations the SRES A1B emissions scenario for greenhouse gases was used. For four simulations the SRES A1B scenario for N_2O was replaced by one of the four Representative Concentration Pathway emissions scenarios for N_2O, while for the other four, the SRES A1B scenario for CH_4 was replaced by one of the four Representative Concentration Pathway emissions scenarios for CH_4. Increases in NO_x-mediated ozone loss resulting from increasing N_2O concentrations lead to a decrease in global-mean total column ozone. Increasing CH_4 concentrations increase the rate of HO_x-mediated ozone loss in the upper stratosphere. Overall however, increasing CH_4 concentrations lead to an increase in global-mean total column ozone. Stratospheric column ozone over the 21st century exhibits a near-linear response to changes in N_2O and CH_4 surface concentrations, which permits a simple parameterisation for the ozone response to changes in the concentrations of these gases.

The results presented in this thesis provide a comprehensive picture of how stratospheric ozone may evolve through the 21st century under a range of greenhouse gas emissions scenarios, and quantitatively extend concepts that had previously been understood only qualitatively.

Publications

Some of the material in chapters of this thesis has previously been published as follows:

- Chapter 3 – Revell, L. E., G. E. Bodeker, D. Smale, R. Lehmann, P. E. Huck, B. E. Williamson, E. Rozanov, and H. Struthers, The effectiveness of N_2O in depleting stratospheric ozone, *Geophys. Res. Lett., 39*(L15806), 2012.

- Chapter 4 – Revell, L. E., G. E. Bodeker, P. E. Huck, and B. E. Williamson, Impacts of the production and consumption of biofuels on stratospheric ozone, *Geophys. Res. Lett., 39*(L10804), 2012.

- Chapter 5 – Revell, L. E., G. E. Bodeker, P. E. Huck, B. E. Williamson, and E. Rozanov, The sensitivity of stratospheric ozone changes through the 21^{st} century to N_2O and CH_4, *Atmos. Chem. Phys. Discussions, 12,* 17583-17605, 2012.

Acknowledgements

Many people have contributed to this thesis through their support, be it scientific, technical, financial or emotional support. I wish to thank the following individuals and organisations:

My PhD supervisors, **Greg Bodeker, Petra Huck and Bryce Williamson** have taught me *a lot* over the last three years, ranging from atmospheric science to computer programming and scientific writing. They each get a huge thank you for being fantastic supervisors. **Dan Smale** taught me how to run the NIWA-SOCOL chemistry-climate model, and ran simulations for me until I was up to speed. **Ralph Lehmann** ran AWI photochemical box model simulations for me, and **Malte Meinshausen** provided me with the MAGICC6 model. In 2011 I visited the University of Maryland, and I am grateful to **Ross Salawitch** and **Tim Canty** for hosting my visit. **NIWA** and **Bodeker Scientific** provided the financial support for me to undertake a PhD. Thanks to NIWA Christchurch for accommodating me for the past three years, and to NIWA Lauder also, on my occasional visits – especially following the devastating Christchurch earthquake in 2011. **Hilary McMillan** and **Emily Lane** from NIWA Christchurch have averted my Matlab crises on several occasions, and together with other colleagues we have enjoyed many tea breaks and bike rides.

I am lucky to have wonderful friends and family in Christchurch, Hamilton and beyond, who have supported me through the PhD journey. Finally, a massive thank you to my loving husband **John Revell**, for everything.

Contents

List of Figures

List of Tables

Glossary

AOGCM atmosphere-ocean general circulation model

AWI Alfred Wegener Institute

CCM chemistry-climate model

CCMVal-2 Chemistry-Climate Model Validation phase 2

CFC chlorofluorocarbon

CMIP3 Coupled Model Intercomparison Project phase 3

C^{4}MIP Coupled Carbon Cycle Climate Model Intercomparison Project

ECHAM5 European Centre Hamburg Model v.5

EESC equivalent effective stratospheric chlorine

GCM general circulation model

GHGs greenhouse gases

GWP global-warming potential

HCFC hydrochlorofluorocarbon

IPCC Intergovernmental Panel on Climate Change

IR infrared

KPP Kinetic Preprocessor

LLNL Lawrence Livermore National Laboratory

MAECHAM4 Middle Atmosphere European Centre Hamburg Model v.4

MAGICC6 Model for the Assessment of Greenhouse Gas Induced Climate Change v.6

MEZON Model for Evaluating ozone trends

MPIOM Max Planck Institute Ocean Model

NIWA National Institute of Water and Atmospheric Research

ODP ozone-depletion potential

ODS ozone-depleting substance

PSC polar stratospheric cloud

RCP representative concentration pathway

SCM simple climate model

SIC sea-ice concentration

SOCOL Solar-Climate Ozone Links

SPARC Stratospheric Processes and their Role in Climate

SRES Special Report on Emissions Scenarios

SST sea-surface temperature

TUV Tropospheric Ultraviolet and Visible

UKMO-HadCM3 United Kingdom Met Office – Hadley Centre Coupled Model v.3

UV ultraviolet

WCRP World Climate Research Programme

WMO World Meteorological Organization

Chemical abbreviations

$Cl_y = Cl + 2\times Cl_2 + ClO + 2\times Cl_2O_2 + ClONO_2 + HCl + HOCl + BrCl$

$HO_x = H + OH + HO_2$

$HO_y = 2\times H_2O + 2\times H_2 + 4\times CH_4 + 2\times CH_2O$

$NO_x = NO + NO_2$

$NO_y = N + NO + NO_2 + NO_3 + 2\times N_2O_5 + HNO_3 + HNO_4 + ClONO_2 + BrONO_2$

Chapter 1

Introduction

Over the last century, human activities have led to vast changes in atmospheric composition. It was initially assumed that atmospheric dilution would prevent pollutants released into the atmosphere from incurring harmful consequences. However phenomena such as photochemical smog and acid rain later proved that anthropogenic interference with the atmosphere can be to the detriment of the biosphere. Furthermore, the harmful effects of atmospheric pollutants are not always felt close to their source. Nowhere is this more evident as in the case of the Antarctic ozone hole, which is caused by chemicals that were emitted predominantly in the Northern Hemisphere.

Atmospheric modelling is necessary to gain an understanding of how anthropogenic activities have changed and will change the Earth's atmosphere. How will emissions of anthropogenic greenhouse gases, which are impacting all areas of the Earth system, affect stratospheric ozone? This was addressed a decade ago by Randeniya et al. [2002], who found that nitrous oxide (N_2O) and methane (CH_4) would lead to decreases in stratospheric ozone through the 21^{st} century. The importance of including the effects of greenhouse gas-induced temperature changes on ozone in such calculations was later pointed out by Chipperfield and Feng [2003]. More recently, Ravishankara et al. [2009] emphasised the important role that N_2O plays in stratospheric ozone depletion by assigning it an ozone-depletion potential. This thesis aims to rigorously evaluate the impacts of N_2O and CH_4 on stratospheric ozone through the use of a state-of-the-art chemistry-climate model.

This chapter introduces fundamental concepts relating to the stratosphere, and of particular relevance to the subject of this thesis. Section 1.1 introduces the structure of the atmosphere, stratospheric chemistry and stratospheric circulation. The ozone layer, a well known and extremely important feature of the stratosphere, is discussed in Section 1.2. Here, processes leading

to the formation of the Antarctic ozone hole are discussed, as well as the Montreal Protocol for Substances that Deplete the Ozone Layer, and the outlook for 21st century ozone. N_2O and CH_4 are likely to play an important role in determining future ozone concentrations, which is the main focus of this thesis, and so their roles as greenhouse gases and ozone-depleting substances are outlined in Section 1.3. Section 1.4 provides an outline for the rest of this thesis.

1.1 The stratosphere

The stratosphere is the region of the atmosphere between approximately 10 and 50 km above Earth's surface (corresponding to a pressure range of approximately 100-1 hPa). Its existence has been known since the early 20th century, when instrumented balloon experiments performed independently by Teisserenc de Bort and Richard Assmann showed that temperature increases with altitude above ∼10 km [*Labitzke and van Loon*, 1999]. As shown in Figure 1.1, the stratosphere is separated from the troposphere below by the tropopause, and from the mesosphere above by the stratopause. Additionally, the stratosphere contains ∼90% of the ozone in the atmosphere (red trace in Figure 1.1), as discussed further in Section 1.2.

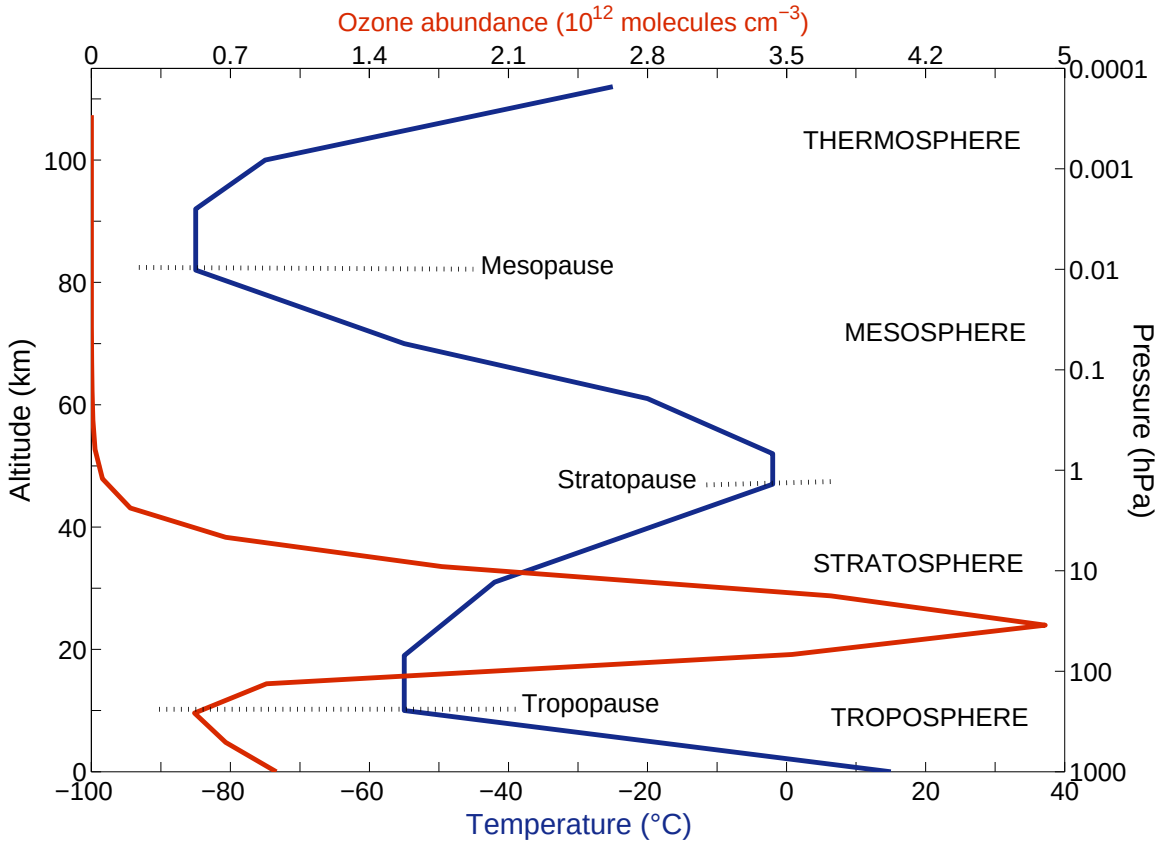

Figure 1.1: *Global-mean air temperature and ozone abundance relative to altitude and pressure. Data taken from Brasseur and Solomon [2005].*

In the classification used in Figure 1.1, the regions of the atmosphere are divided according to temperature (blue trace), and whether it increases or decreases with altitude. The major energy source for the Earth's atmosphere is solar radiation, and it is the fate of that radiation, along with the physical and chemical processes it induces, that determine the temperature profile shown in Figure 1.1.

The solar spectrum is usually categorised into five spectral windows: infrared (IR) (700 nm-1 mm), visible (400-700 nm) and three bands within the ultraviolet (UV) region: UV-A (320-400 nm), UV-B (280-320 nm) and UV-C (250-280 nm) [*Brasseur and Solomon*, 2005]. UV-C radiation is damaging to life in the biosphere, but is absorbed by N_2 and O_2, the dominant gases in Earth's atmosphere. UV-B radiation is strongly absorbed by ozone in the stratosphere. However, anthropogenic depletion of the ozone layer through the 20^{th} century is correlated with increased UV-B flux to the biosphere over that same period, contributing to increased rates of skin cancer, eye diseases and DNA damage. Radiation in the UV-A and visible ranges is partially absorbed by trace constituents, reflected or scattered. Much of it reaches Earth's surface where it is essential to much of life in the biosphere. IR radiation is emitted and absorbed by Earth's surface and greenhouse gases (GHGs) in the atmosphere [*Brasseur and Solomon*, 2005].

Absorption of solar radiation by Earth's surface heats the lower layers of the troposphere, meaning that temperature decreases with altitude in the troposphere. In addition, rising parcels of air expand and cool at lower pressures. In the stratosphere, temperature increases with increasing altitude due to the absorption of UV-B radiation by ozone. In the mesosphere, temperature again decreases with altitude, due to decreased solar heating and cooling caused by emission of IR radiation from GHGs in the stratosphere. Lastly, temperature increases with altitude in the thermosphere due to absorption of solar radiation by N_2 and O_2 [*Dessler*, 2000; *Jacobson*, 2005].

Increased concentrations of GHGs are associated with a net trapping of heat in the troposphere. This is known as the greenhouse effect, and without it the Earth would be too cold to support the life forms that currently inhabit it. Increases in GHG concentrations have caused the Earth's average surface temperature to increase by 0.51 °C since mid-20^{th} century (http://www.nasa.gov/topics/earth/features/2011-temps.html).

Although the troposphere is warming, the stratosphere is cooling. This is because GHGs in the stratosphere emit heat to space, and this cooling effect exceeds the absorption of IR radiation in the stratosphere. Additionally, absorption of IR radiation in the stratosphere is decreasing because increasing amounts of GHGs in the troposphere trap IR radiation lower down in the atmosphere. The net effect is cooling [*Manabe and Wetherald*, 1975].

The effects of GHGs on the climate system can be compared and quantified by a number of metrics. Below are some definitions of parameters referred to throughout this thesis.

- **Radiative forcing** is defined by *Forster et al.* [2007] as: "The change in net (down minus up) irradiance (solar plus longwave; in W m^{-2}) at the tropopause after allowing for stratospheric temperatures to readjust to radiative equilibrium, but with surface and tropospheric temperatures and state held fixed at the unperturbed values." This essentially means that when the Earth system is at equilibrium, the energy going in and out through the tropopause is balanced. When GHG abundances increase, less energy leaves the troposphere, due to the greenhouse effect. The additional heating caused to the troposphere while the Earth system adjusts to its new equilibrium is the radiative forcing. Radiative forcing provides a simple metric for ranking and quantifying the effects of long-lived GHGs on climate.

- A GHG's **global-warming potential (GWP)** is based on its global-mean radiative forcing resulting from a 1 kg pulse emission, relative to the radiative forcing resulting from a 1 kg pulse emission of CO_2, and integrated over some time horizon (often 100 years) [*Forster et al.*, 2007].

- **Lifetimes** refer to the time taken to reduce the abundance of a chemical species in the atmosphere to $\frac{1}{e}$ of its original value [*Brasseur and Solomon*, 2005].

1.1.1 Atmospheric chemistry

The atmosphere is in a constant state of flux. Changes in temperature, solar zenith angle and the concentrations of chemical species, amongst other factors, all affect the rate at which chemical reactions occur. It is important to be able to calculate these changing reaction rates so that chemical processes can be modelled accurately. Classes of reactions that commonly occur in the stratosphere are described below. Further details are given in *Atkins* [1998]; *Dessler* [2000], and *Brasseur and Solomon* [2005]. Reactions of particular importance to this thesis are listed in Appendix A.

Photolysis reactions occur when a molecule is split by the absorption of light. For example:

$$O_2 + h\nu \longrightarrow O + O \tag{1.1}$$

The rate of Reaction 1.1 is calculated according to:

$$\text{Rate} = J[O_2] \tag{1.2}$$

where $[O_2]$ is the oxygen concentration, and J the photolysis frequency (in units of s^{-1}). J, in

turn, is calculated using the solar actinic flux (number of photons available (photons cm^{-2} s^{-1} nm^{-1})), the absorption cross-section (the effective probability of the O_2 molecule absorbing a photon in units of cm^2), and the quantum yield for photodissociation (the dimensionless probability of photon absorption leading to decomposition of the O_2 molecule) [*Brasseur and Solomon*, 2005].

Bimolecular reactions involve the collision of two species, for example:

$$NO + O_3 \longrightarrow NO_2 + O_2 \tag{1.3}$$

The rate for this reaction is calculated as:

$$\text{Rate} = k[NO][O_3] \tag{1.4}$$

where k is the rate constant, which is generally temperature dependent, according to the Arrhenius equation:

$$k = Ae^{-E_a/RT} \tag{1.5}$$

The pre-exponential factor A (cm^3 $molecule^{-1}$ s^{-1}) represents the total frequency of collisions in which the reactants are in the correct molecular configuration for a reaction to occur. The exponential part, $e^{-E_a/RT}$, represents the proportion of such collisions that results in a successful reaction (forms the specified products); E_a (J mol^{-1}) is the activation energy for the reaction (normally taken to represent the minimum kinetic energy that the reactants must have in order to react); R denotes the universal gas constant (8.314 J mol^{-1} K^{-1}), and T the absolute temperature (K).

Three-body reactions occur when two species collide with a third body to form a product, for example:

$$O + O_2 + M \longrightarrow O_3 + M \tag{1.6}$$

In the terrestrial atmosphere, the third body, denoted M, is usually N_2 or O_2 (since they are the most common molecules) and remains chemically unaltered by the reaction. Its role is essentially to carry away any excess energy to allow the product to relax to a stable, bound state. Since the concentration of M changes with pressure, the rate constant for three-body reactions depends on both temperature and pressure.

Complex reactions involve more than one elementary step. The Arrenhius equation usually applies for two- and three-body reactions, and for elementary, single-step reactions, E_a is

generally greater than zero. Consequently, the vast majority of reactions speed up with increasing temperature. For most complex (multi-step) reactions, the Arrenhius equation still generally applies. But E_a is now an effective parameter; and furthermore, it is not restricted to a value greater than zero. In fact for several reactions important to the work in this thesis (for example, Reaction 3.4), E_a is less than zero, which means, counter-intuitively, that the reactions accelerate at lower temperatures. Because the stratosphere is projected to continue cooling in future (associated with increasing GHG concentrations), this is an important consideration for 21^{st} century stratospheric chemistry.

Heterogeneous reactions occur on the surfaces of liquid or solid particles, such as sulfate aerosols and polar stratospheric clouds (PSCs). PSCs are condensed phases of H_2O, HNO_3 and/or H_2SO_4. For example, the complex Reaction 1.7 (below) begins with the adsorption of H_2O onto a PSC particle. $ClONO_2$ collides with the particle, to produce HOCl and HNO_3. HOCl is then photolysed to form OH and Cl radicals (Reaction 1.8), thus forming an efficient pathway for conversion of the reservoir species $ClONO_2$ into active chlorine (capable of participating in ozone-depleting catalytic cycles).

$$ClONO_2 + H_2O \longrightarrow HOCl + HNO_3 \tag{1.7}$$

$$HOCl + h\nu \longrightarrow OH + Cl \tag{1.8}$$

Reaction 1.7 is much faster as a heterogeneous reaction than the corresponding bimolecular gas-phase reaction [*Brasseur and Solomon*, 2005]. Its rate depends on the thermal velocity of the $ClONO_2$ molecules, the PSC particle surface-area density, and the reactive uptake coefficient (proportion of collisions between $ClONO_2$ and the PSC particle that lead to the indicated products).

1.1.2 Stratospheric circulation

A parcel of air can move in three dimensions: vertical, zonal (east-west directions) and meridional (north-south). Stratospheric **zonal circulation** is caused by meridional temperature gradients and is strong, meaning that air is well mixed in the zonal direction [*Holton*, 2004]. **Vertical circulation** is weaker than the zonal or meridional circulations in terms of mass flux, and, along with the meridional circulation, is generated by stratospheric wave forcing and diabetic heating and cooling [*Dessler*, 2000].

The overall **meridional circulation** is called the Brewer-Dobson circulation, proposed independently by Alan Brewer and Gordon Dobson in 1949 and 1956, respectively [*Brasseur and Solomon*, 2005]. In the Brewer-Dobson circulation, deep convection causes air from the tropical troposphere to ascend into the stratosphere, where it is transported towards the poles, and descends in middle and polar latitudes [*Forster et al.*, 2011]. By this mechanism, chlorine compounds historically produced from chlorofluorocarbons (CFCs), predominantly emitted in the Northern Hemisphere, were transported to the Antarctic stratosphere, leading to the development of the Antarctic ozone hole (Section 1.2.2) [*Farman et al.*, 1985; *McElroy et al.*, 1986; *Solomon et al.*, 1986]. Chemistry-climate model simulations of the future evolution of the atmosphere project that the Brewer-Dobson circulation is to strengthen throughout the 21st century [*Butchart et al.*, 2010]. This is due to stronger extra-tropical planetary waves originating from the troposphere, caused in turn by increasing sea-surface temperatures (SSTs) as a result of climate change [*Butchart and Scaife*, 2001; *Fomichev et al.*, 2007]. The result is enhanced transport of gases to polar regions, but also shorter stratospheric residence times of chemical constituents, affecting the lifetimes of long-lived GHGs [*Cook and Roscoe*, 2012].

1.2 The ozone layer

Approximately 99% of the molecules in the stratosphere are either N_2 or O_2. The rest are a mixture of trace gases, one of which is ozone (O_3). Around 90% of atmospheric ozone lies between 100 and 1 hPa (approximately 10-50 km), leading to the term "the ozone layer" (Figure 1.1). Ozone has a very large absorption cross-section for UV photons and absorbs solar UV radiation that is harmful to terrestrial organisms. As seen in Figure 1.1, some ozone also exists in the troposphere as the result of reactions between hydrocarbon and nitrogen oxide gases, produced (for example) as a result of fossil fuel combustion. Tropospheric ozone is an air pollutant and contributes towards respiratory problems in humans [*West et al.*, 2007].

1.2.1 Chapman chemistry

A series of mechanisms to explain the production and destruction of atmospheric ozone was first proposed by *Chapman* [1930], and is now known as the Chapman cycle. The cycle begins with O_2 photolysis to produce two oxygen atoms:

$$O_2 + h\nu \longrightarrow O + O \tag{1.9}$$

Atomic oxygen undergoes a three-body reaction with O_2 in what is the dominant ozone production process in the stratosphere:

$$O + O_2 + M \longrightarrow O_3 + M \tag{1.10}$$

The resulting ozone can be photolysed, producing atomic oxygen either in its ground state ($O(^3P)$, also referred to hereafter as O) or in a metastable excited state ($O(^1D)$), depending on the wavelength of the incident photon:

$$O_3 + h\nu \longrightarrow O_2 + O(^3P) \quad \lambda \gtrsim 320 \text{ nm} \tag{1.11}$$

$$O_3 + h\nu \longrightarrow O_2 + O(^1D) \quad \lambda \lesssim 320 \text{ nm} \tag{1.12}$$

Despite being short-lived, $O(^1D)$ is highly reactive and is present in sufficient concentration to play a crucial role in upper-stratospheric chemistry. It is deactivated to ground state atomic oxygen via molecular collisions:

$$O(^1D) + M \longrightarrow O + M \tag{1.13}$$

Finally, atomic oxygen and ozone can react to produce O_2:

$$O + O_3 \longrightarrow 2O_2 \tag{1.14}$$

Because Chapman chemistry alone cannot quantitatively account for the amount of ozone present in the stratosphere (e.g., Section 5.2 of *Seinfeld and Pandis* [2006]), it became apparent through the 20$^{\text{th}}$ century that reactions involving hydrogen-oxide and nitrogen-oxide radicals are important in determining the 'natural' balance of stratospheric ozone [*Bates and Nicolet*, 1950; *Crutzen*, 1970]. Such reactions are discussed in Section 1.3. Towards the end of the 20$^{\text{th}}$ century, it also became increasingly clear that the ozone layer was under threat from anthropogenic emissions of halogen-containing hydrocarbons (halocarbons), which lead to chlorine- and bromine-catalysed ozone depletion, and severe polar ozone loss.

1.2.2 Antarctic ozone loss

By the 1970s, halocarbons were in widespread industrial use as refrigerants, aerosol propellants, and in many other applications. Common halocarbons are the CFCs, hydrochlorofluorocarbons (HCFCs) and halons (brominated haloalkanes). Halocarbon applications took advantage of the chemicals' low toxicity and low reactivity. But because of their low reactivity, *Molina and Rowland* [1974] theorized that the main sink for the halocarbons must be the stratosphere,

where they could undergo UV photolysis leading to accelerated ozone destruction.

In 1985, *Farman et al.* [1985] published total column ozone measurements from Halley Bay indicating a substantial decrease in October mean Antarctic ozone. Spatial averages of satellite-based measurements of Antarctic total column ozone in October (Figure 1.2) show the steep decline in ozone observed through the late 20$^{\text{th}}$ century. Year-to-year variability is caused by temperature fluctuations; the Antarctic stratosphere in 1988 was anomalously warm [*Kanzawa and Kawaguchi*, 1990], while in 2002 the Antarctic polar vortex split in two, which led to surprisingly low ozone depletion [*Hoppel et al.*, 2003]. Figure 1.2 also shows Arctic polar-cap average total column ozone in March, which is discussed further on in this section.

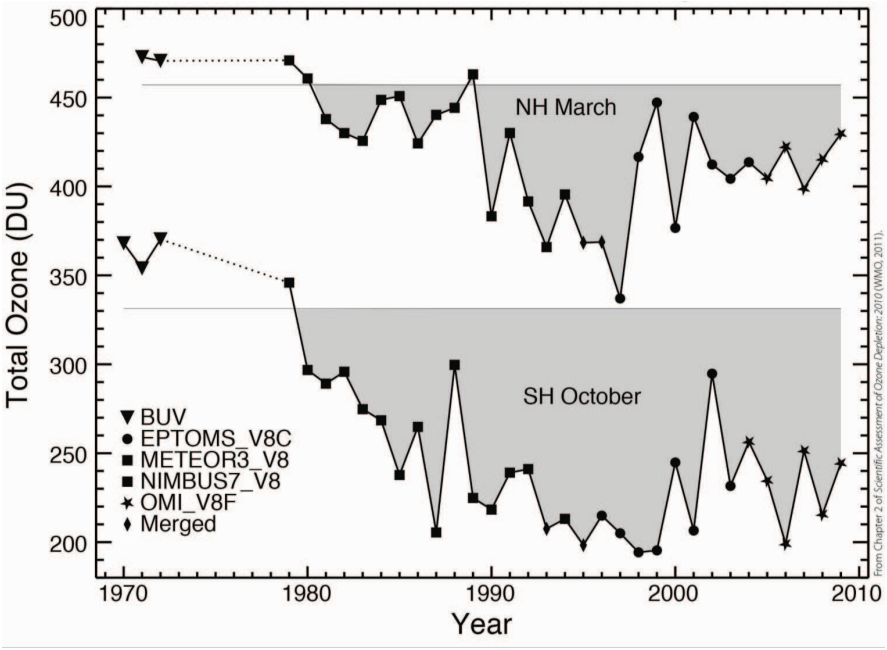

Figure 1.2: *Total ozone satellite measurements averaged over 63-90°N in March and over 63-90°S in October. Horizontal lines represent average ozone for the years before 1983. Different symbols indicate data from different satellites. 1988 and 2002 were anomalous years, as explained in the text. Source: [Douglass et al., 2011].*

The processes leading to the formation of the ozone hole begin with photolysis of halocarbons in the stratosphere (where UV light is more intense than in the troposphere). Chlorine or bromine atoms so released then participate in upper-stratospheric gas-phase ozone-loss cycles,

for example (X = Cl or Br):

$$\begin{aligned} \mathrm{X} + \mathrm{O_3} &\longrightarrow \mathrm{XO} + \mathrm{O_2} \\ \mathbf{XO} + \mathbf{O} &\longrightarrow \mathbf{X} + \mathbf{O_2} \\ \hline \mathrm{O} + \mathrm{O_3} &\longrightarrow 2\mathrm{O_2} \end{aligned}$$

Alternatively, Cl (or Br) atoms may form the reservoir gases HCl (or HBr) and $\mathrm{ClONO_2}$ (or $\mathrm{BrONO_2}$) [*Stolarski and Cicerone*, 1974; *Wofsy et al.*, 1975; *Rowland et al.*, 1976], which are transported poleward by the Brewer-Dobson circulation. Due to differences in hemispheric circulation patterns, the Antarctic stratosphere gets much colder than the Arctic stratosphere during winter months. Such cold Antarctic stratospheric temperatures facilitate the formation of PSCs, containing condensed ice and aerosol particles. Heterogeneous reactions on the surfaces of PSCs convert halogen reservoir gases into active chlorine and bromine during winter [*Salawitch et al.*, 1993]. Over the winter months, active species, particularly involving chlorine, accumulate within the polar vortex (a circumpolar flow that forms in the Antarctic winter troposphere/stratosphere), which prevents air from moving into and out of the Antarctic stratosphere.

When sunlight returns to Antarctic latitudes in late winter/early spring, the following photocatalytic cycles may be initiated (with rate-determining steps shown in bold) [*McElroy et al.*, 1986; *Molina and Molina*, 1987]:

Cycle XI:

$$\begin{aligned} 2\mathrm{ClO} + \mathrm{M} &\longrightarrow \mathrm{Cl_2O_2} + \mathrm{M} \\ \mathbf{Cl_2O_2} + \mathbf{h\nu} &\longrightarrow \mathbf{ClO_2} + \mathbf{Cl} \\ \mathrm{ClO_2} + \mathrm{M} &\longrightarrow \mathrm{Cl} + \mathrm{O_2} + \mathrm{M} \\ 2(\mathrm{Cl} + \mathrm{O_3} &\longrightarrow \mathrm{ClO} + \mathrm{O_2}) \\ \hline 2\mathrm{O_3} &\longrightarrow 3\mathrm{O_2} \end{aligned}$$

Cycle XVb:

$$\begin{aligned} \mathbf{BrO} + \mathbf{ClO} &\longrightarrow \mathbf{BrCl} + \mathbf{O_2} \\ \mathrm{BrCl} + \mathrm{h\nu} &\longrightarrow \mathrm{Br} + \mathrm{Cl} \\ \mathrm{Br} + \mathrm{O_3} &\longrightarrow \mathrm{BrO} + \mathrm{O_2} \\ \mathrm{Cl} + \mathrm{O_3} &\longrightarrow \mathrm{ClO} + \mathrm{O_2} \\ \hline 2\mathrm{O_3} &\longrightarrow 3\mathrm{O_2} \end{aligned}$$

This sudden activity in late winter/early spring causes the ozone depletion phenomenon commonly referred to as the "ozone hole." As the polar vortex breaks up, the ozone-depleted air

migrates north and the ozone hole is dissipated.

Inter-hemispheric circulation differences mean that the Arctic winter stratosphere is warmer and more disturbed than the Antarctic winter stratosphere [*Solomon et al.*, 2007]. This means that the volume of PSCs in the Arctic stratosphere is less and so Arctic ozone loss is not usually as severe as it is in the Antarctic. However in 2011, ozone depletion during the Arctic winter/spring period was comparable with that observed in the Antarctic [*Manney et al.*, 2011]. This was because high-latitude Arctic stratospheric temperatures were unusually cold for a prolonged period, which led to a greater volume of PSCs, and thereby enhanced chemical ozone destruction.

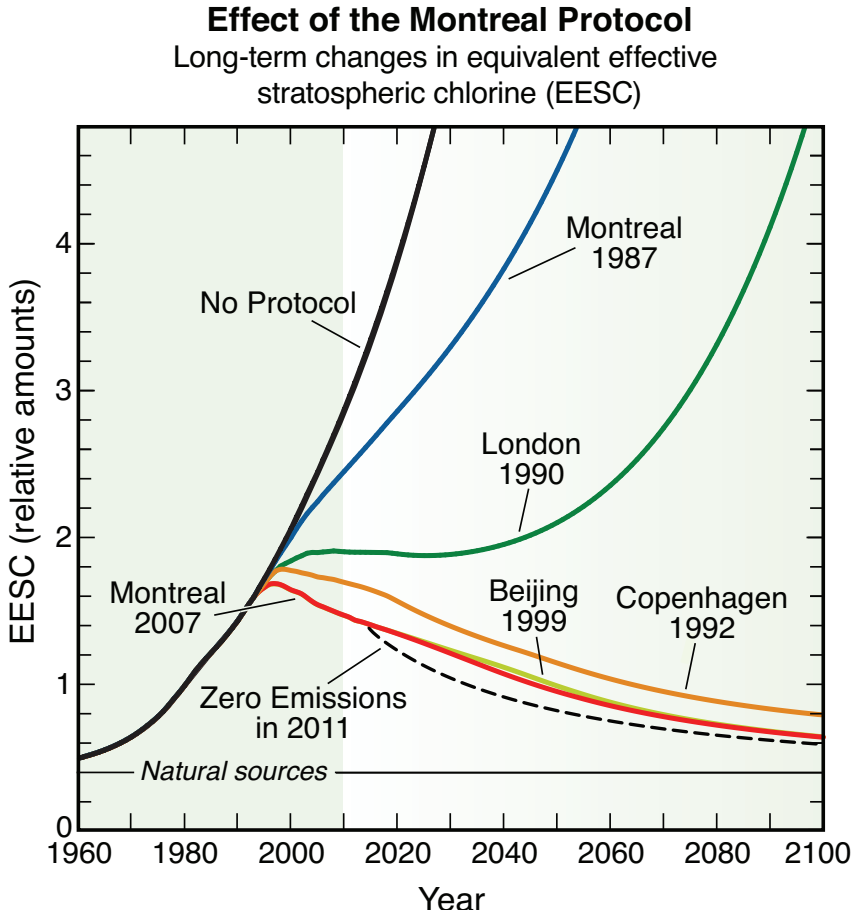

Figure 1.3: *Midlatitude projections of EESC showing the effect of the Montreal Protocol, subsequent amendments, the case where ODSs had never been regulated, and the case where emissions ceased entirely beginning in 2011. Source: [WMO, 2010].*

1.2.3 The Montreal Protocol and 21st century ozone

Owing to widespread concern over the effects of halocarbons on stratospheric ozone, a protocol was designed to phase-out the production and consumption of ozone-depleting sub-

stances (ODSs). Called the Montreal Protocol for Substances that Deplete the Ozone Layer, it was signed on the 16th of September 1987. Amendments to the Protocol were later made in London (1990), Copenhagen (1992), Beijing (1999) and Montreal (2007). The Protocol has now been ratified by all 196 United Nations member countries [*WMO*, 2010]. Figure 1.3 shows the projected effects of the Montreal Protocol and later amendments on equivalent effective stratospheric chlorine (EESC) over the period up to 2100. EESC is a measure of the potential of chlorine and bromine in an air mass to destroy ozone, and takes into account the fact that bromine is more effective than chlorine on a per-atom basis [*Daniel et al.*, 2011].

As shown in Figure 1.3, the Copenhagen 1992 and subsequent amendments mean that EESC is now projected to decrease over the 21st century, towards a level approaching that which would be expected had emissions entirely ceased beginning in 2011. In contrast to these projections, a chemistry-climate model (CCM) study by *Newman et al.* [2009] suggested that if ODSs had not been regulated, and if their production had increased by 3% each year, 67% of global-mean column ozone (relative to 1980 values) would have been depleted by 2065.

As well as benefitting the ozone layer, and hence life on Earth, the Montreal Protocol has benefitted the climate, since most ODSs are also GHGs. Indeed, in terms of reducing radiative forcing, the Montreal Protocol has already contributed more to the amelioration of anthropogenic climate change than will be achieved by the reduction target of the first commitment period of the Kyoto Protocol (an international agreement aimed at reducing anthropogenic GHG emissions) [*Velders et al.*, 2007].

Global-mean stratospheric ozone is projected to increase in the 21st century, for two reasons:

1. Halogen concentrations will continue to decrease due to the Montreal Protocol and its amendments, as shown by the Montreal 2007 trace in Figure 1.3. Therefore, chlorine- and bromine-catalysed ozone depletion is projected to slow over the 21st century [*Bekki et al.*, 2011].

2. The stratosphere is projected to continue cooling with increasing GHG concentrations, which leads to an increase in ozone abundances [*Rosenfield et al.*, 2002; *Jonsson et al.*, 2004]. The Chapman cycle reactions 1.10 and 1.14 are highly temperature-dependent; The rate of Reaction 1.10 increases with decreasing temperature, while Reaction 1.14 slows with decreasing temperature.

CCM projections of 21st century ozone follow in Section 2.3.5.

1.3 Greenhouse gases and ozone

CO_2, the dominant anthropogenic GHG, does not chemically react with ozone. It affects ozone indirectly via stratospheric cooling, as described above. In terms of radiative forcing, the two dominant GHGs after CO_2 controlled by the Kyoto Protocol are CH_4 and N_2O. Radiative forcings and GWPs for these gases are shown in Table 1.1. Tropospheric ozone and halocarbons each exert greater radiative forcings than N_2O (0.35 W m^{-2} and 0.337 W m^{-2} respectively [*Forster et al.*, 2007]), but are not controlled under the Kyoto Protocol. N_2O and CH_4 both break down in the stratosphere to produce reactive nitrogen- and hydrogen-containing species that participate in ozone-depleting catalytic cycles. Such processes are described in Sections 1.3.1 and 1.3.2.

Table 1.1: *GHG radiative forcings and GWPs [Forster et al., 2007].*

	Radiative forcing (W m^{-2})	100-year GWP
CO_2	1.66	1
CH_4	0.48	25
N_2O	0.16	298

1.3.1 Nitrous oxide (N_2O)

N_2O is long-lived, with an atmospheric lifetime of approximately 114 years in the stratosphere [*Forster et al.*, 2007], and has both natural and anthropogenic sources (e.g., Table 2.5 of *Seinfeld and Pandis* [2006]). Natural sources include tropical soils and the oceans (due to microbial activity), whereas anthropogenic sources include industrial processes and agriculture – in particular the use of nitrogen-based fertilizers [*Montzka et al.*, 2011]. The atmosphere's N_2O concentration has increased from 276 ppb to 322 ppb since pre-industrial times [*Montzka et al.*, 2011], and is projected to continue increasing through the 21st century. Therefore we can expect that, in future, N_2O will have a greater impact on climate (in terms of radiative forcing), and on ozone (as will now be discussed).

The major sink for N_2O is in the stratosphere, where it is photolysed or oxidised via the following three reactions [*Dessler*, 2000]:

$$N_2O + h\nu \longrightarrow N_2 + O \tag{1.15}$$

$$N_2O + O(^1D) \longrightarrow 2NO \tag{1.16}$$

$$N_2O + O(^1D) \longrightarrow N_2 + O_2 \tag{1.17}$$

Most N_2O (around 90%) is destroyed by photolysis (Reaction 1.15). Although it is not a major breakdown path for N_2O, Reaction 1.16 is very important to ozone chemistry because it produces NO. The nitrogen oxides NO and NO_2 are collectively referred to as NO_x, and Reaction 1.16 is the major source of stratospheric NO_x.

In the stratosphere, NO_x radicals catalytically deplete ozone [*Crutzen*, 1970] via the cycles shown below:

Cycle I:

$$\begin{aligned} NO + O_3 &\longrightarrow NO_2 + O_2 \\ \mathbf{NO_2 + O} &\longrightarrow \mathbf{NO + O_2} \\ \hline O_3 + O &\longrightarrow 2O_2 \end{aligned}$$

Cycle II:

$$\begin{aligned} NO + O_3 &\longrightarrow NO_2 + O_2 \\ NO_2 + O_3 &\longrightarrow NO_3 + O_2 \\ \mathbf{NO_3 + h\nu} &\longrightarrow \mathbf{NO + O_2} \\ \hline 2O_3 &\longrightarrow 3O_2 \end{aligned}$$

The destructive effect of NO_x on ozone first became a concern in the 1970s, when Boeing proposed building a fleet of supersonic transport aircraft that would fly in the stratosphere [*Crutzen*, 1971; *Johnston*, 1971; *McElroy and McConnell*, 1971]. This, and other environmental concerns, along with political and economic factors, led to the project eventually being cancelled [*Staehelin et al.*, 2001].

Now that CFC production has been phased out under the Montreal Protocol, N_2O emissions are expected to be the dominant emissions of ODSs through the 21st century (although currently they deplete less ozone than do the CFCs, owing to the long stratospheric lifetime of CFCs) [*Ravishankara et al.*, 2009]. The impact of N_2O on ozone in the 21st century is the subject of Chapter 3.

Finally, concerns over the ozone-depleting impacts of N_2O and NO_x have been raised in regard to increased biofuels production and consumption [*Crutzen et al.*, 2008]. Because nitrogen-based

fertilizers are applied to crops intended for use as biofuels, N_2O emissions are projected to increase as global crop production increases. This topic will be discussed in further detail in Chapter 4.

1.3.2 Methane (CH_4)

Natural sources of CH_4 include wetlands, termites and the oceans; anthropogenic sources include landfills, biomass burning, agriculture and waste disposal [*Wuebbles and Hayhoe*, 2002]. Since pre-industrial times, atmospheric CH_4 has increased from 700 ppb to around 1800 ppb [*Seinfeld and Pandis*, 2006; *Montzka et al.*, 2011]. CH_4 has a lifetime of 9 years [*Montzka et al.*, 2011], which is much shorter than N_2O's lifetime.

CH_4 oxidation by $O(^1D)$ forms OH [*Dessler*, 2000]:

$$CH_4 + O(^1D) \longrightarrow CH_3 + OH \tag{1.18}$$

OH radicals then undergo other gas-phase reactions, interconverting to H atoms and HO_2 radicals. Collectively, H, OH and HO_2 are referred to as HO_x. HO_x radicals participate in ozone-depleting catalytic cycles, such as Cycle V shown below and Cycles IV-VIII listed in Appendix A. These cycles are particularly prevalent in the upper stratosphere, where HO_x concentrations are maximized.

Cycle V:

$$\begin{aligned} OH + O_3 &\longrightarrow HO_2 + O_2 \\ \mathbf{HO_2 + O} &\longrightarrow \mathbf{OH + O_2} \\ \hline O_3 + O &\longrightarrow 2O_2 \end{aligned}$$

One important difference in CH_4's behaviour in the stratosphere in comparison with N_2O's is that, as well as *depleting* ozone, CH_4 can lead to *increases* in ozone via the reduction of ozone depletion by other pathways. Two mechanisms explain how this occurs [*Portmann and Solomon*, 2007; *Fleming et al.*, 2011]:

1. CH_4 reacts with Cl to form HCl (Reaction 1.19), thus 'tying up' active chlorine as reservoir chlorine and thereby ameliorating the ozone-depleting activity of Cl.

$$CH_4 + Cl \longrightarrow CH_3 + HCl \tag{1.19}$$

2. CH_4 produces HO_x radicals (as previously discussed), the main loss process for which is

formation of water vapour via:

$$OH + HO_2 \longrightarrow H_2O + O_2 \tag{1.20}$$

In turn, water vapour cools the stratosphere, thereby slowing ozone depletion by the gas-phase ozone-loss cycles (see Section 1.2.3).

CH_4 is lost primarily by reaction with OH:

$$CH_4 + OH \longrightarrow CH_3 + H_2O \tag{1.21}$$

OH reacts with many atmospheric species, such as GHGs and other pollutants, and so plays an important role in determining GHG lifetimes. Indeed, *Manning and Reisinger* [2011] showed that OH has played a larger role in reducing radiative forcing associated with climate change than the carbon cycle has over the past 50 years. Future increases in temperature and humidity (as a result of climate change), reduced UV flux to the troposphere (as a result of stratospheric ozone increases), as well as emissions of NO_x, CO, CH_4 and other hydrocarbons, will serve to alter the global distribution and abundance of OH [*Denman et al.*, 2007].

1.4 Thesis structure

Chapter 2 describes photochemical box models, simple climate models and chemistry-climate models; the numerical models that were used to obtain the results presented in Chapters 3, 4 and 5 (the research chapters). Chapter 3 investigates the effectiveness of N_2O as an ODS through the 21st century. Chapter 4 examines the effects that GHG changes resulting from increased biofuels production and consumption could have on the ozone layer. In Chapter 5, the results from an investigation into the sensitivity of ozone to CH_4 and N_2O are presented. Final conclusions and future outlook are summarised in Chapter 6.

Chapter 2

Computational methods

Given that it is impossible (and potentially dangerous) to perform controlled experiments on Earth's atmosphere as a whole, numerical models of atmospheric processes are necessary to evaluate the impact of any anthropogenic interventions. Depending on the applications for which they were designed, models differ in the processes they represent, spatial and temporal scales, complexity, and consequently the computing power required to run them. This chapter introduces and describes the models that were used for the studies presented in Chapters 3 to 5: the AWI photochemical box model, MAGICC6 simple climate model and NIWA-SOCOL chemistry-climate model. The chapter concludes with descriptions of the halocarbon and greenhouse gas emissions scenarios used in the modelling work presented in this thesis.

2.1 Photochemical box models

Photochemical box models simulate chemical processes within a box, assumed to be sufficiently small that all chemical concentrations are homogeneous within it. They are relatively simple models, requiring little computer memory or computing time for multi-year simulations. This makes them useful for applications such as analysing measurements of atmospheric species [*Brasseur et al.*, 2003], or quantifying contributions to ozone loss from different chemical families, as described in Chapter 3.

Box models encompass a prescribed set of chemical reactions, and calculate changes in concentrations for all species involved in that set of reactions. Rate coefficients are included as input data, and initial conditions are prescribed. Chemical reaction pathways are combined to form a set of coupled differential equations which are then solved numerically. Because the lifetimes of individual gases vary by orders of magnitude, not all numerical methods are able to accurately solve the differential equations unless a very small time step is used; in addition, the numerical solver must be stable and mass-conserving [*Jacobson*, 2005]. Dynamical processes are not explicitly represented in photochemical box models. Box models can be constructed to assume a fixed position in the atmosphere, where chemical species can enter and exit the box, or to simulate a parcel of air moving along a trajectory [*Jacobson*, 2005].

As part of the work undertaken for this thesis, a zero-dimensional photochemical box model was developed to study ozone destruction chemistry in the upper stratosphere. It was written in Matlab, and used the multistep implicit-explicit method to solve coupled differential equations [*Jacobson*, 2005]. The gas-phase reactions simulated were the same as those in the National Institute of Water and Atmospheric Research (NIWA)-Solar-Climate Ozone Links (SOCOL) CCM, and rate constants were taken from *Sander et al.* [2006, 2009]. Photolysis rates were calculated using the Tropospheric Ultraviolet and Visible (TUV) model [*Madronich and Flocke*, 1999]. However, when it came to publishing results, the Alfred Wegener Institute (AWI) box model was used in preference to the in-house developed model because of its established track record and international credibility.

The AWI photochemical box model simulates 175 reactions between 48 chemical species in the stratosphere [*Krämer et al.*, 2003; *Wohltmann et al.*, 2010]. It is based on modules for gas-phase chemistry [*Brasseur et al.*, 1997], heterogeneous chemistry [*Carslaw et al.*, 1995], and photolysis (TUV by *Madronich and Flocke* [1999]). Rate constants were taken from the compilations given by *Sander et al.* [2006, 2009]. Differential equations are generated and solved numerically by the

Kinetic Preprocessor (KPP), a software tool that simulates chemical reaction systems [*Damian et al.*, 2002].

For the simulations performed for Chapter 3, the AWI box model assumed a fixed position in the atmosphere. This approach neglects the zonal circulation, which means that the length of day for the 'box' of air is slightly modified. However for the latitude and altitude range of interest (2°N and 1 to 5 hPa), this has a negligible effect on the chemistry investigated.

2.2 The MAGICC6 simple climate model

Climate change is frequently studied with atmosphere-ocean general circulation models (AOGCMs), which are complex three-dimensional models of physical, radiative and dynamical processes in the atmosphere coupled to an ocean model [*Brasseur and Solomon*, 2005]. However because AOGCMs are computationally expensive, simple climate models (SCMs) were developed to complement AOGCMs and are better suited for some studies. SCMs are designed to emulate AOGCMs; processes simulated by AOGCMs are parameterised within SCMs so that simulations take little time to run. SCMs can also be used to isolate sources of uncertainties in AOGCMs [*Meinshausen et al.*, 2011a].

The Model for the Assessment of Greenhouse Gas Induced Climate Change v.6 (MAGICC6) SCM consists of a carbon cycle model and a hemispherically averaged ocean model coupled to an atmosphere layer. The carbon cycle model is globally averaged, the ocean model in each hemisphere has 40 layers, and the atmosphere model includes land and ocean boxes in each hemisphere [*Meinshausen et al.*, 2011a].

MAGICC6 can be calibrated to emulate any of the 10 Coupled Carbon Cycle Climate Model Intercomparison Project (C^4MIP) carbon cycle models and 19 Coupled Model Intercomparison Project phase 3 (CMIP3) AOGCMs, as described by *Meinshausen et al.* [2011a, b]. Climate response parameters in MAGICC6 such as heat exchange coefficients between the land and ocean, and between the hemispheres; climate sensitivity (the warming resulting from CO_2 doubling), and the land-ocean warming ratio, are adjusted to reproduce AOGCM land and ocean time series. Parameters such as the atmospheric CO_2 concentration, carbon pools and carbon fluxes are adjusted to calibrate the carbon cycle model component of MAGICC6.

MAGICC6 can be used to generate projections of global-mean temperature and sea level rise, as was done in the Fourth Assessment Report of the Intergovernmental Panel on Climate

Change (IPCC) [*Randall et al.*, 2007]. MAGICC6 can also generate projections of GHGs for prescribed emissions, described in Chapter 4. Here, it is used to calculate GHG emissions scenarios and to convert emissions to concentrations, which were then used as input to CCM simulations. In Chapter 5, MAGICC6 is used to produce SST series for a range of emissions scenarios. For both studies (Chapters 4 and 5), MAGICC6 was calibrated to the European Centre Hamburg Model v.5 (ECHAM5)/Max Planck Institute Ocean Model (MPIOM) AOGCM core model parameters, and Lawrence Livermore National Laboratory (LLNL) model carbon cycle parameters. These models were chosen for calibration as they gave the best representation of SST and GHG concentration time series that had been used in previous CCM simulations performed for this thesis.

2.3 Chemistry-climate models

CCMs are general circulation models (GCMs) that have been interactively coupled to a detailed chemistry scheme. A dynamical core (the GCM) describes the time evolution of winds, temperature and pressure, based on parameterisations and simulations of key physical processes such as radiation, convection, transport and chemistry [*Morgenstern et al.*, 2010]. Chemistry and dynamics are coupled: chemical processes change the chemical composition of the atmosphere, which affects radiative heating and consequently dynamics. Furthermore, dynamical processes affect chemistry via temperature and transport. A schematic of the processes simulated by CCMs is shown in Figure 2.1.

CCMs are computationally very expensive; either high performance computing facilities are required, or for CCMs that can run on a desktop processor (such as the NIWA-SOCOL CCM, Section 2.3.1), multi-decadal simulations must run over the course of several months. CCMs are much more complex models than photochemical box models and SCMs, and are currently the best available tool for simulating the long-term evolution of the global atmosphere.

2.3.1 The NIWA-SOCOL chemistry-climate model

The NIWA-SOCOL CCM is a modified version of the SOCOL model [*Egorova et al.*, 2005; *Schraner et al.*, 2008]. A chemical cycle diagnostic has been implemented in NIWA-SOCOL (described in Section 2.3.2), allowing the attribution of stratospheric odd-oxygen loss to a prescribed set of catalytic cycles.

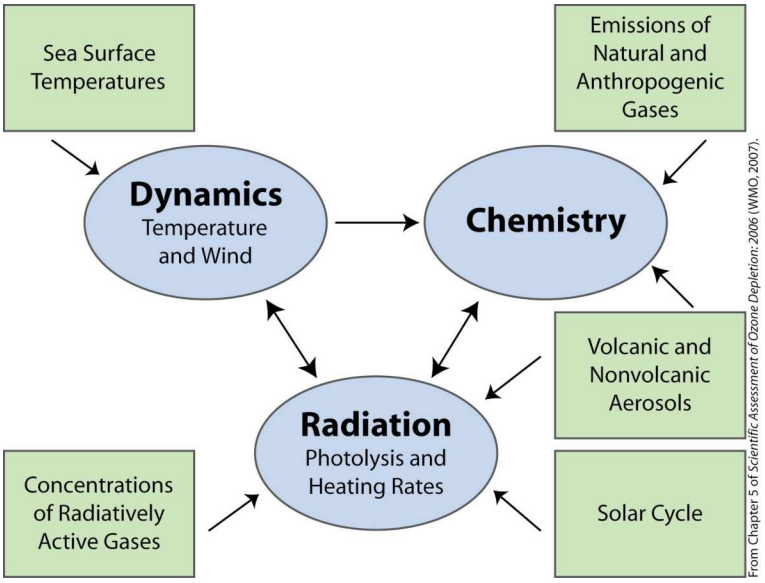

Figure 2.1: *Schematic of a chemistry-climate model. Ovals represent the core of the CCM, boxes represent external impacts and arrows indicate the direction of the effect. Source: [Baldwin et al., 2007].*

NIWA-SOCOL comprises the Middle Atmosphere European Centre Hamburg Model v.4 (MAECHAM4) GCM [*Manzini et al.*, 1997] and the Model for Evaluating ozone trends (MEZON) chemistry transport model [*Egorova et al.*, 2003]. MAECHAM4 is configured with a T31 spectral horizontal resolution (approximately $3.75^\circ \times 3.75^\circ$ grid spacing) and 39 vertical levels between Earth's surface and 0.01 hPa (∼80 km). A hybrid transport scheme [*Zubov et al.*, 1999] is employed to advect the chemical constituents whilst the chemical solver algorithm uses a Newton-Raphson iterative method taking into account 41 chemical species, 140 gas-phase reactions, 46 photolysis reactions and 16 heterogeneous reactions. A 15-minute time step is used for dynamical processes while radiative and chemical calculations are performed every two hours. Photolysis rates are calculated online, meaning that they are calculated during the simulation, taking into account pressure, solar zenith angle, overhead column ozone, temperature, cloudiness, albedo and solar output [*Rozanov et al.*, 1999; *Eyring et al.*, 2010a].

NIWA-SOCOL was used to study the sensitivity of stratospheric ozone changes to future GHG emissions and the results are presented in Chapters 3 to 5.

2.3.2 Attribution of odd-oxygen loss in NIWA-SOCOL

NIWA-SOCOL attributes odd-oxygen loss to 15 catalytic cycles, as well as the odd-oxygen Chapman cycle (Section 1.2.1), using a diagnostic approach similar to that employed by *Lee et al.* [2002]. The diagnostic implemented in NIWA-SOCOL differs from that used by *Lee et al.*

[2002] in that it does not employ a passive tracer to advect odd-oxygen, and tracks a larger set of catalytic cycles. The cycles tracked by NIWA-SOCOL, listed in Appendix A, were chosen to form a general diagnostic set that can be used for a range of studies.

Within each model grid cell, changes in the odd-oxygen ($O + O(^1D) + O_3$) removal rates (in molecules cm^{-3} s^{-1}) are calculated using the rate-limiting steps of the corresponding reaction cycles. For example, the rate-determining step of Cycle IX below is highlighted in bold:

Cycle IX:

$$\begin{aligned} Cl + O_3 &\longrightarrow ClO + O_2 \\ \mathbf{ClO + O} &\mathbf{\longrightarrow Cl + O_2} \\ \hline O_3 + O &\longrightarrow 2O_2 \end{aligned}$$

Odd-oxygen loss (L) attributed to Cycle IX is calculated as follows:

$$L_{IX} = -2k[ClO][O] \tag{2.1}$$

where k is the rate constant for the rate-determining step of Cycle IX; L_{IX} is negative because the reaction leads to loss of odd-oxygen, and the factor of two appears because Cycle IX leads to the net destruction of two molecules of odd-oxygen (one of O_3 and one of O). At each time step, the odd-oxygen changes due to chemistry and net transport, as well as the total odd-oxygen change, are logged in each grid cell, allowing attribution of ozone changes through that time step to chemical or dynamical origins.

2.3.3 CCMVal-2

The World Climate Research Programme (WCRP) Stratospheric Processes and their Role in Climate (SPARC) Chemistry-Climate Model Validation phase 2 (CCMVal-2) activity was undertaken to improve scientific understanding of CCMs through process-oriented evaluation [*Eyring et al.*, 2010a]. 18 modelling groups, including the NIWA-SOCOL group, contributed simulations to CCMVal-2. This enabled model strengths and flaws to be highlighted through model-to-model and model/observations comparisons, and projections of future stratospheric ozone to be made.

As described in the SPARC CCMVal-2 report [*Eyring et al.*, 2010a], NIWA-SOCOL has a good representation of global-mean temperatures in the upper and middle stratosphere, but less so in the lower stratosphere. The Brewer-Dobson circulation is overly strong, and dates of return

of ozone to 1980 values are too early, due to an enhanced reduction in stratospheric chlorine. Within CCMVal-2, photolysis rates, fast (radical) chemistry, long-lived (reservoir) chemistry and polar chemistry were evaluated to assess the performance of the models' chemistry schemes. NIWA-SOCOL performed well in the comparison of photolysis rates, but the fast chemistry was not evaluated because certain files were not submitted to the CCMVal-2 archive during the time the evaluations were conducted. Overall, NIWA-SOCOL performed soundly in the evaluation of long-lived chemistry; it simulates the correlation between different chemical tracers well, indicating that both chemical and transport processes are well represented in the model. A notable exception is the NO_y vs. N_2O correlation, which indicates that too much N_2O is lost as NO_y (compared with the other loss pathways outlined in Section 1.3.1). Polar chemical ozone loss is simulated satisfactorily in the Antarctic, but less so in the Arctic. Although the NIWA-SOCOL model has some shortcomings, the absolute values of chemical constituent mixing ratios do not need to be correct for the studies presented in Chapters 3 to 5 because the relative (rather than absolute) changes in stratospheric chemistry are analysed.

2.3.4 REF-B2 boundary conditions

The NIWA-SOCOL simulations analysed in Chapters 3 to 5 are based on a so-called "REF-B2" simulation performed for the WCRP SPARC CCMVal-2 activity [*Eyring et al.*, 2010a]. REF-B2 simulations were designed to encompass the period 1960-2100, and include only anthropogenic forcings (natural forcings, such as volcanic eruptions, were excluded because they are not known for the future). CO_2, CH_4 and N_2O follow the IPCC Special Report on Emissions Scenarios (SRES) A1B scenario for GHGs, and ODSs follow the adjusted A1 scenario for halocarbons (Section 2.4). SSTs and sea-ice concentrations (SICs) are prescribed using output from GCM simulations adhering to the SRES A1B scenario [*Morgenstern et al.*, 2010].

2.3.5 CCM projections of 21st century ozone

REF-B2 CCM simulations from the CCMVal-2 activity show that, except in the tropical lower stratosphere, ozone increases everywhere throughout the 21st century due to decreasing concentrations of stratospheric chlorine and bromine, and CO_2-induced stratospheric cooling. As an example, Northern Hemisphere annual-mean midlatitude ozone is shown in Figure 2.2. Tropical lower-stratospheric ozone is projected to decrease because the rate of tropical upwelling is expected to increase, leaving less time for ozone to form in rising parcels of ozone-poor air from the troposphere to the stratosphere [*Avallone and Prather*, 1996; *Eyring et al.*, 2007]. Multi-model mean results from the CCMVal-2 assessment indicate that global-mean column ozone

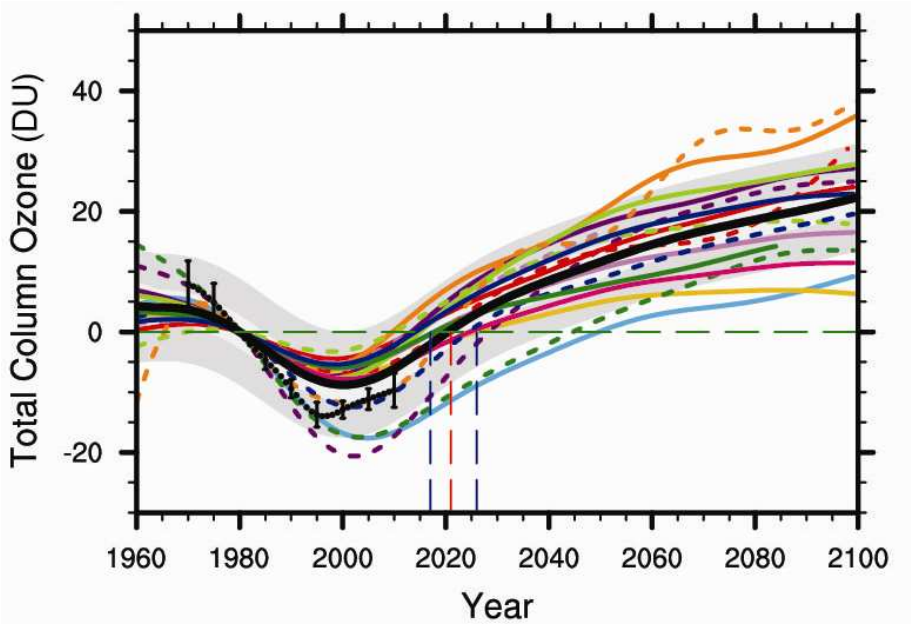

Figure 2.2: *Northern Hemisphere annual-mean total column ozone (35-60°N), for observations (black dots) and CCM projections, adjusted to the 1980 baseline. The light green dashed trace represents the NIWA-SOCOL CCM, and shows that this model simulates a return of ozone to the 1980 baseline in ∼2010. Total ozone observations were calculated from four data sets: ground-based measurements, merged satellite data, the NIWA combined total column ozone database, and Solar Backscatter Ultraviolet retrievals. Source: [Bekki et al., 2011].*

may return to 1980 values in ∼2032, and 1960 values in ∼2053 [*Eyring et al.*, 2010a; *Bekki et al.*, 2011].

2.4 Emissions scenarios

The **adjusted A1 scenario for halocarbons** reflects the phase-out of ODSs legislated under the Montreal Protocol for Substances that Deplete the Ozone Layer and later amendments [*Daniel et al.*, 2007]. It is 'adjusted,' because, at the 2007 meeting of the Parties to the Protocol, an earlier phase-out of HCFCs was agreed upon. Mixing ratios for CFC-11, CFC-12, halon-1211 and halon-1301 under this scenario are shown in Figure 2.3. The adjusted A1 scenario was the current baseline scenario for halocarbons at the time that the CCM simulations analysed in Chapters 3 to 5 were initiated, however that scenario has now been superseded by the publication of the 2010 World Meteorological Organization (WMO) Scientific Assessment of Ozone Depletion [*Daniel et al.*, 2011]. The new scenario for halocarbons is similar to the previous one, although some discrepancies occur – for example when changes have occurred regarding

reported production of halocarbons, or assumptions about future emissions.

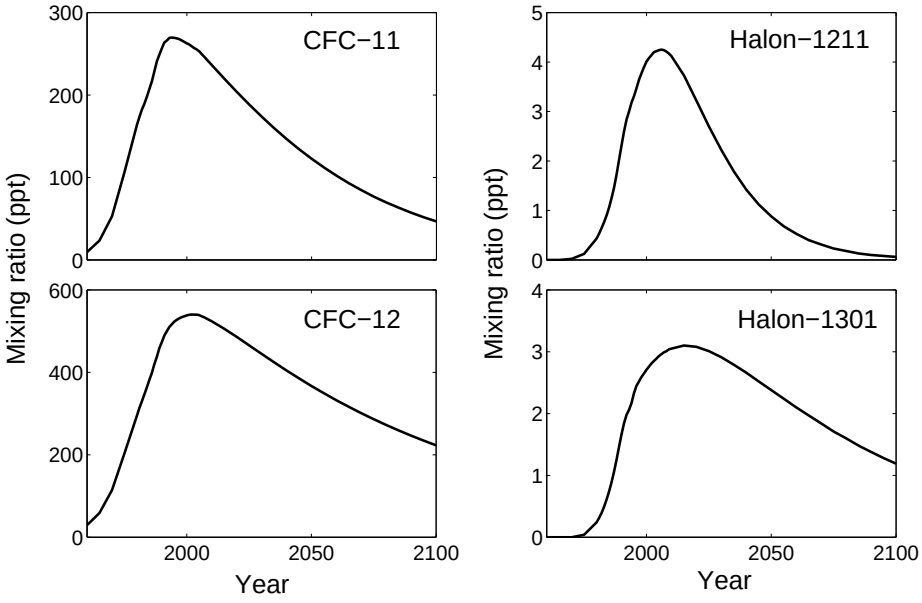

Figure 2.3: *Mixing ratios of selected ODSs under the adjusted A1 scenario for halocarbons.*

Within the **IPCC SRES** scenario group, the SRES A1B and B1 scenarios for GHGs portray intermediate and relatively small increases in anthropogenic radiative forcing, respectively. SRES A1B reflects rapid growth in the international economy and global population that peaks around 2050 then declines. It assumes rapid introduction of new technologies that use a balance of energy sources based on fossil and non-fossil fuels. SRES B1 represents efforts to mitigate GHG emissions through sustainable development and environmental consciousness [*Nakicenovic and Swart*, 2001]. CO_2, N_2O and CH_4 surface concentrations under the SRES A1B and B1 scenarios are shown in Figure 4.1.

The IPCC SRES scenarios are being superseded by a new set of scenarios that encompass socio-economic, emission and climate projections. The **representative concentration pathways (RCPs)** are the first step towards the development of these scenarios [*van Vuuren et al.*, 2011]. The RCPs were developed for the climate modelling community, and provide possible concentration trajectories for the main climate change forcing agents. There are four RCPs: 2.6, 4.5, 6.0 and 8.5, named according to the radiative forcings (in W m^{-2}) reached by 2100. N_2O and CH_4 concentrations for the RCPs are shown in Figure 5.1.

Chapter 3

The effectiveness of N_2O in depleting stratospheric ozone

With emissions of chlorine- and bromine-containing ODSs being phased out under the Montreal Protocol for Substances that Deplete the Ozone Layer, N_2O is projected to be the dominant substance responsible for ozone depletion emitted in the 21^{st} century [Ravishankara et al., 2009]. As emissions of anthropogenic GHGs increase through the 21^{st} century, the dynamical, chemical and radiative properties of the stratosphere are expected to change, and these will change the efficiency of N_2O as an ODS. Here, a CCM simulation of an evolving atmosphere was run from 1960-2100 to examine the effects of the Montreal Protocol, and anthropogenic climate change, on N_2O-induced ozone depletion.

3.1 Introduction

In the stratosphere, reaction of N_2O with $O(^1D)$ leads to the production of NO by Reaction 3.1:

$$N_2O + O(^1D) \longrightarrow 2NO \tag{3.1}$$

NO subsequently undergoes various reactions to form stratospheric reservoir nitrogen (NO_y = N + NO + NO_2 + NO_3 + 2×N_2O_5 + HNO_3 + HNO_4 + $ClONO_2$ + $BrONO_2$) [*Brasseur and Solomon*, 2005]. NO is also one of the reactive nitrogen oxides (NO_x), participating in ozone-depleting catalytic cycles, as discussed in Section 1.3.1 [*Crutzen*, 1970]. N_2O is the primary source of stratospheric NO_x [*McElroy and McConnell*, 1971], and therefore can affect stratospheric ozone [*Randeniya et al.*, 2002]. Indeed, of all the anthropogenic substances currently emitted, N_2O is projected to be the dominant contributor to ozone depletion through the 21st century [*Ravishankara et al.*, 2009].

The effect of NO_x on stratospheric ozone is moderated by dynamical, chemical and radiative processes. The principal dynamical process affecting NO_x production from N_2O is the Brewer-Dobson circulation (see Section 1.1.2). Throughout the 21st century, the Brewer-Dobson circulation is projected to strengthen due to increasing SSTs [*Fomichev et al.*, 2007]. A strengthening Brewer-Dobson circulation increases the rate at which air is transported through the stratosphere, and therefore increases the rate at which NO_y is removed from the stratosphere [*Cook and Roscoe*, 2012].

Chemical factors influencing the effect of NO_x on ozone include the concentration of reservoir chlorine, Cl_y (Cl + 2×Cl_2 + ClO + 2×Cl_2O_2 + $ClONO_2$ + HCl + HOCl + BrCl). Since the reaction of NO_2 with ClO forms $ClONO_2$, when the concentration of reservoir chlorine is high, more $ClONO_2$ is formed at the expense of NO_x [*Ravishankara et al.*, 2009; *Fleming et al.*, 2011].

The radiative environment of the stratosphere is projected to change through the 21st century as increasing CO_2 concentrations cool the stratosphere (Section 1.1). The concentration of NO_y decreases as the stratosphere cools because the NO_y sink is temperature-dependent; cooling slows Reaction 3.2 (below), and the resulting increase in N increases the rate of Reaction 3.3 [*Rosenfield and Douglass*, 1998]. Therefore, more NO_y is converted to molecular nitrogen (N_2). As a result, decreasing stratospheric temperatures are projected to slow ozone depletion by NO_x [*Randeniya et al.*, 2002; *Chipperfield and Feng*, 2003].

$$N + O_2 \longrightarrow NO + O \tag{3.2}$$

$$N + NO \longrightarrow N_2 + O \tag{3.3}$$

Previous CCM studies, using the same boundary conditions as used in this chapter, modelled the effect of CO_2-induced stratospheric cooling on N_2O and revealed that while N_2O remains an important gas for ozone depletion through the 21st century, its effects are mitigated by stratospheric cooling [*Oman et al.*, 2010; *Plummer et al.*, 2010]. In a more recent CCM study, *Fleming et al.* [2011] removed the effect of CO_2-induced stratospheric cooling by keeping all GHG concentrations (other than N_2O) constant. Without stratospheric cooling, they found that the increase in N_2O concentrations led to a decrease in global annual-mean total column ozone of ∼6 DU between 1960 and 2100.

For the work presented in this chapter, a CCM simulation of an evolving atmosphere was used to examine ozone-depleting NO_x chemistry, and how it is altered by changes in the chemical, dynamical and radiative properties of the stratosphere.

3.2 Computational methods

A NIWA-SOCOL CCM simulation was performed from 1950-2100, with the first ten years treated as a spin-up period. The simulation conformed to REF-B2 boundary conditions (Section 2.3.4), and used the adjusted A1 scenario for halocarbons and IPCC SRES A1B scenario for GHGs. Chemical box model calculations were performed using the AWI box model. Details of the models and emissions scenarios used are given in Chapter 2.

3.3 Results and discussion

Global annual-mean column ozone is projected to increase through the 21st century, due to stratospheric cooling [*Rosenfield et al.*, 2002] and the phase-out of halogenated ODSs under the Montreal Protocol. NIWA-SOCOL simulates an increase in global annual-mean column ozone of 5.5 DU between 1960 and 2100, compared with the multi-model mean increase of 4 DU simulated by the CCMVal-2 models [*Bekki et al.*, 2011]. The larger ozone increase simulated by NIWA-SOCOL is caused by that model's overly strong Brewer-Dobson circulation, and a larger-than-average reduction in stratospheric Cl_y (see e.g. Figure 9.24 of *Eyring et al.* [2010a]).

While global-mean column ozone is projected to increase, N_2O continues to play an important role in ozone depletion through the 21st century. Under the SRES A1B emissions scenario, N_2O emissions lead to a 27% increase in surface N_2O concentrations from 1960 to 2100. In a non-changing climate, we would expect a proportionate increase in NO_x, and also in the strength of the NO_x ozone-loss cycles. Of these cycles, NIWA-SOCOL diagnostics show that Cycle I (below), for which the rate-determining step is Reaction 3.4, accounts for >99% of NO_x-induced ozone depletion:

Cycle I:

$$\begin{aligned} NO + O_3 &\longrightarrow NO_2 + O_2 \\ \mathbf{NO_2 + O} &\longrightarrow \mathbf{NO + O_2} \\ \hline O_3 + O &\longrightarrow 2O_2 \end{aligned} \tag{3.4}$$

Figure 3.1(a) shows the zonal-mean rate of Cycle I averaged over the 2090s decade, relative to the 1960s decade. The strength of Cycle I increases up to 4% in the tropical upper stratosphere (red region), which is not as much as might be expected given the 27% increase in surface N_2O concentrations. Elsewhere, the rate of Cycle I slows between 1960 and 2100 (up to 40% in the tropical lower stratosphere).

What causes the general slowing of the rate of Cycle I in the stratosphere? Because NIWA-SOCOL simulates an evolving atmosphere, changes in stratospheric circulation, chemistry and temperature alter the ratios NO_y/N_2O, NO_x/NO_y and NO_2/NO, all of which affect the concentration of NO_2 (required in Reaction 3.4), and therefore the rate at which Cycle I can proceed. The time series of these three ratios are plotted in Figures 3.1(b-d) as global annual means, normalised to the 1960-1969 mean.

The NO_y/N_2O ratio decreases from 1960 to 2100 (Figure 3.1(b)), indicating that the strengthening Brewer-Dobson circulation increases the mass flux of NO_y out of the stratosphere [*Cook and Roscoe*, 2012]. In addition, stratospheric cooling decreases NO_y [*Rosenfield and Douglass*, 1998], which contributes further to the decrease in NO_y/N_2O. The NO_x/NO_y ratio decreases at altitudes below ~7 hPa between 1960 and 2100 (Figure 3.1(c)) because stratospheric cooling and increasing concentrations of reactive hydrogen (HO_x) lead to an increase in the rate of Reaction 3.5:

$$NO_2 + OH + M \longrightarrow HNO_3 + M \tag{3.5}$$

Within the NO_x family, NO_2 and NO are in equilibrium throughout the stratosphere during daytime, and interconvert primarily by Cycle I, NO_2 photolysis and Reaction 3.6 [*Brasseur and*

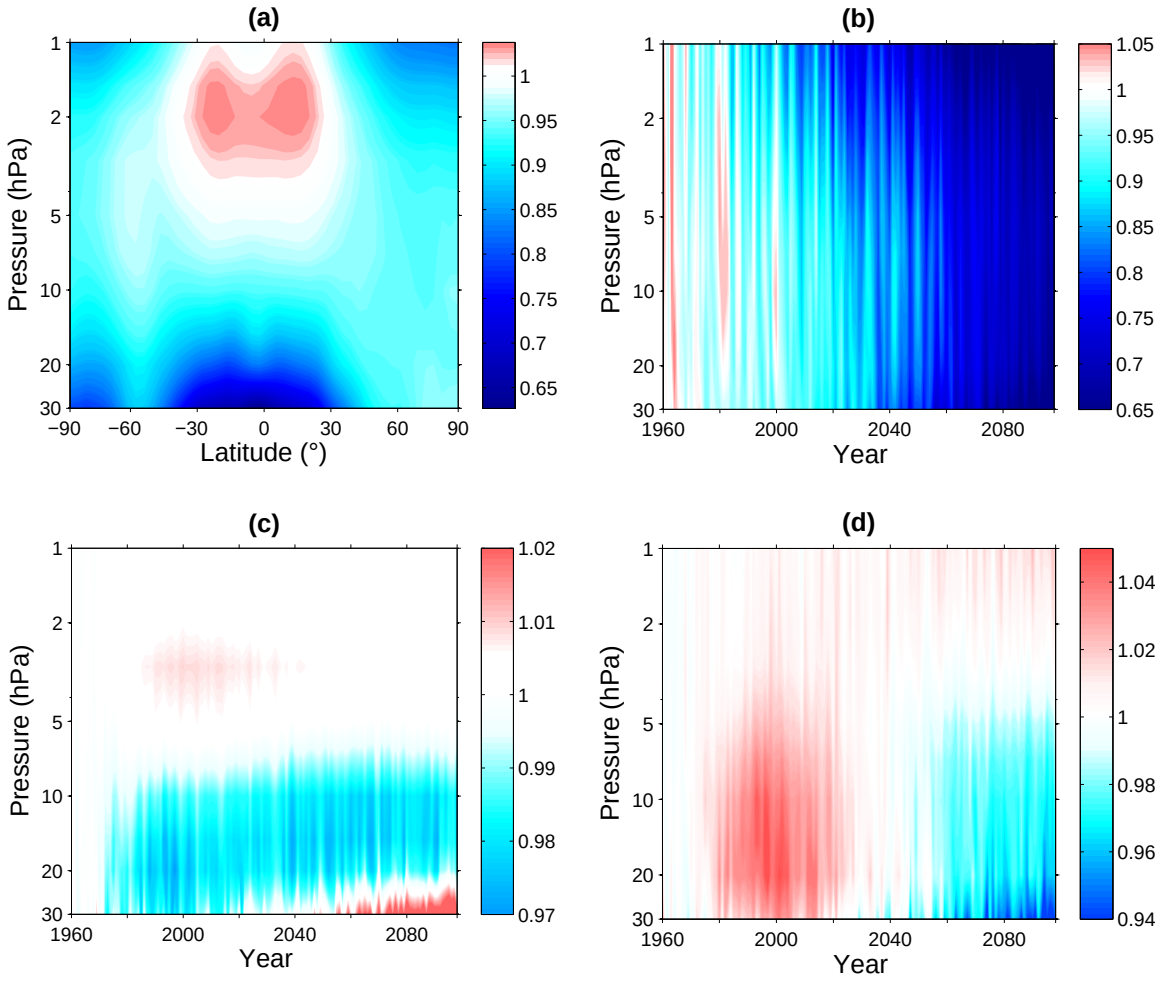

Figure 3.1: *(a) 2090s zonal-mean rate of Cycle I (molecules cm^{-3} s^{-1}) normalised to the 1960s mean, displayed as a function of pressure and latitude; (b) Global annual-mean ratio of NO_y/N_2O normalised to the 1960-1969 mean, displayed as a function of pressure and time; (c) Same as (b) but for NO_x/NO_y; (d) Same as (b) but for NO_2/NO.*

Solomon, 2005]:

$$NO + ClO \longrightarrow NO_2 + Cl \tag{3.6}$$

Figure 3.1(d) shows that the NO_2/NO ratio increases from 1960 to ~2000, and then decreases through the 21st century. The simulated increase in NO_2/NO between 1960 and 2000 is due to increased chlorine loading (as a result of halocarbon emissions), which increases the rate of Reaction 3.6. Conversely, between 2000 and 2100, the decreasing concentration of ClO slows Reaction 3.6, decreasing the NO_2/NO ratio. Additional decreases in the NO_2/NO ratio through the 21st century are caused by CO_2-induced stratospheric cooling, which slows the temperature-dependent first step of Cycle I.

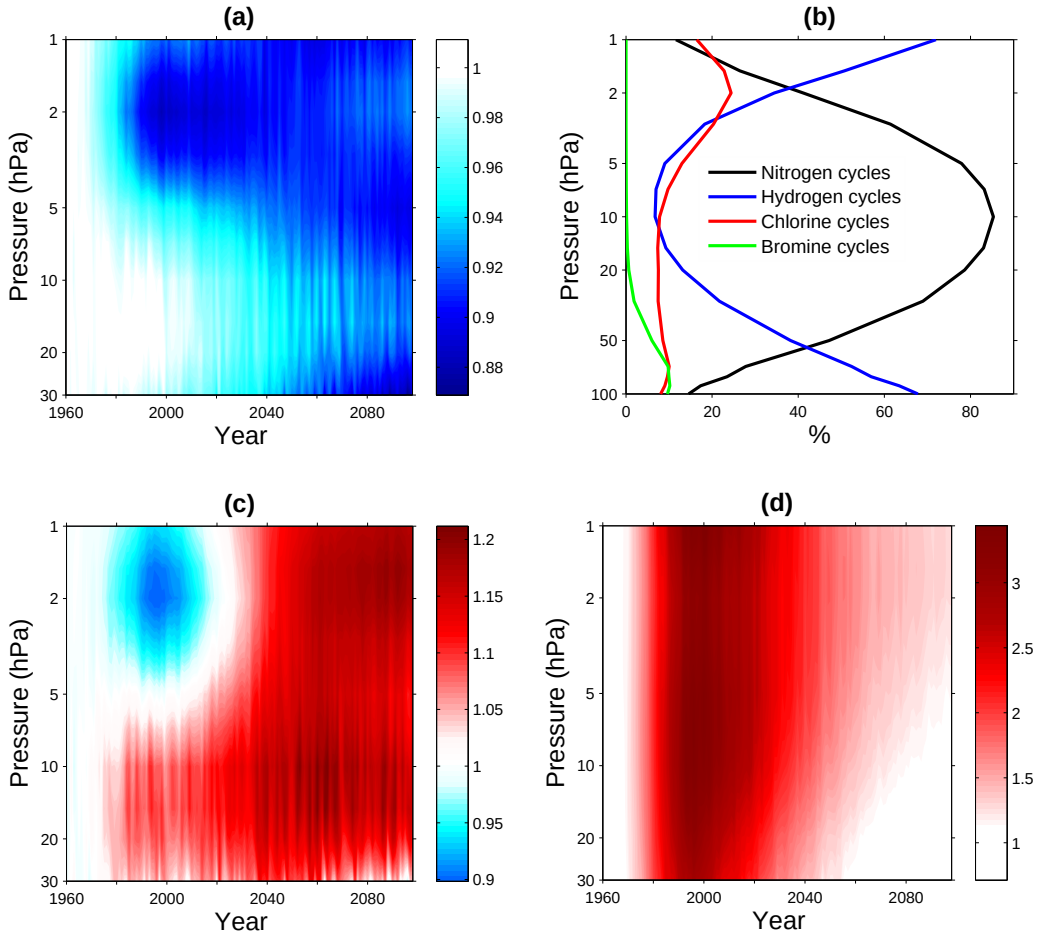

Figure 3.2: *(a) The global annual-mean rate of Cycle I (molecules cm^{-3} s^{-1}) divided by the global annual-mean abundance of NO_2 (molecules cm^{-3}) and normalised to the 1960-1969 mean; (b) Percentage contributions to global-mean ozone loss from 15 catalytic ozone-loss cycles tracked by NIWA-SOCOL, averaged over 1960-2100. Cycles are shown in Appendix A and grouped as follows: Nitrogen cycles (I-III); hydrogen cycles (IV-VIII); chlorine cycles (IX-XIII); bromine cycles (XIV-XV); (c) The global annual-mean rate of the hydrogen cycles, normalised to the 1960-1969 mean; (d) Same as (c), but for the chlorine cycles.*

Through the 21st century, the NO_y/N_2O, NO_x/NO_y and NO_2/NO ratios exhibit a general decrease between 1 and 30 hPa (the region of interest), which leads to smaller NO_2 concentrations than might be expected on the basis of the increase in surface N_2O concentrations. Because NO_2 is required in the rate-determining step of cycle I (Reaction 3.4), smaller-than-expected NO_2 concentrations must be at least partially responsible for the slowing rate of Cycle I observed through most of the stratosphere. To test whether they are entirely responsible, the rate of Cycle I is divided by the NO_2 concentration.

The rate of Reaction 3.4, which is the rate-determining step of Cycle I, is $R_I = k_3[NO_2][O]$. Dividing R_I by $[NO_2]$ therefore allows the effects of k_3 and [O] on the strength of Cycle I to be examined. This quantity (normalised to the 1960-1969 mean) is plotted in Figure 3.2(a), which

shows that $R_I/[NO_2]$ decreases throughout the stratosphere over the 21st century indicating that either k_3 or [O] (or both) has decreased significantly over that period. However, k_3 has a negative activation energy [*Sander et al.*, 2006] and will increase with stratospheric cooling. Consequently, the results displayed in Figure 3.2(a) cannot be explained by the behaviour of k_3 and therefore the reduction of $R_I/[NO_2]$ is due to diminished [O], as simulated by NIWA-SOCOL.

Stratospheric odd-oxygen loss occurs via catalytic cycles commonly involving nitrogen, hydrogen, chlorine or bromine-containing species. Figure 3.2(b) shows the percentage contribution to global-mean ozone loss averaged over the period 1960-2100 from 15 ozone-loss cycles tracked in NIWA-SOCOL, grouped into nitrogen, hydrogen, chlorine and bromine families. The nitrogen cycles dominate in the middle and upper stratosphere, and their combined contribution maximizes at 10 hPa. Chlorine and hydrogen cycles are also important in the upper stratosphere while bromine cycle contributions maximize in the lower stratosphere. Of the five hydrogen and five chlorine cycles tracked in NIWA-SOCOL, the dominant contributors to ozone loss from each family are Cycles V and IX (respectively), shown below. Within the hydrogen family, Cycle V is the dominant contributor to ozone loss in the upper stratosphere (the region of interest), while Cycle IV dominates at lower altitudes (see Appendix A).

Cycle V:

$$\begin{aligned} OH + O_3 &\longrightarrow HO_2 + O_2 \\ \mathbf{HO_2 + O} &\longrightarrow \mathbf{OH + O_2} \\ \hline O_3 + O &\longrightarrow 2O_2 \end{aligned}$$

Cycle IX:

$$\begin{aligned} Cl + O_3 &\longrightarrow ClO + O_2 \\ \mathbf{ClO + O} &\longrightarrow \mathbf{Cl + O_2} \\ \hline O_3 + O &\longrightarrow 2O_2 \end{aligned}$$

Increasing CH_4 emissions to mid-21st century lead to increased concentrations of HO_x (see Section 1.3.2 and *Wuebbles and Hayhoe* [2002]), which enhances ozone loss due to the hydrogen cycles (Figure 3.2(c)). The projected decrease in stratospheric chlorine concentrations owing to the phase-out of halocarbons under the Montreal Protocol results in a slowing of ozone loss due to the chlorine cycles (Figure 3.2(d)). Although these cycles are described as "ozone-loss" cycles, they also lead to overall depletion of other odd-oxygen species since the concentrations of O_3, O and $O(^1D)$ are closely linked. Some cycles (such as the HO_2+O and ClO+O cycles shown above) deplete O directly.

Within the odd-oxygen family, the O/O_3 ratio is projected to decrease over the 21st century because CO_2-induced stratospheric cooling increases the rate of Reaction 3.7 [*Jonsson et al.*, 2004]:

$$O + O_2 + M \longrightarrow O_3 + M \tag{3.7}$$

Here the hypothesis is presented that, in addition to the effect of stratospheric cooling on O/O_3, the concentration of O decreases as a result of the strengthening hydrogen and chlorine cycles in the upper stratosphere, and that this decrease is partially responsible for the slowing rate of Cycle I. To test the effects of reservoir hydrogen (HO_y = 2×H_2O + 2×H_2 + 4×CH_4 + 2×CH_2O) and Cl_y on upper-stratospheric odd-oxygen, box model simulations were performed for the equatorial upper stratosphere (between 1 and 5 hPa), where the odd-oxygen lifetime is sufficiently short to warrant such an analysis.

Five box model simulations (Section 2.1) were performed at 2°N and at 1, 2 and 5 hPa over the period 1960-2100. The first series constituted the 'reference' simulations, in which all parameters (temperature, overhead column ozone and chemical species concentrations) were allowed to vary from decade to decade. In the other four series, one out of temperature, HO_y, Cl_y or overhead column ozone was fixed, and all others varied from decade to decade. Initial concentrations, overhead column ozone, and temperature for these runs were taken from outputs from the NIWA-SOCOL simulation. The box model simulated 10 days from each decade (sufficient time for the box model to reach a steady state), and Figure 3.3 shows the resultant O and O_3 abundance, along with the O/O_3 ratio on the 10th day for the three pressure levels, normalised to 1960.

Figures 3.3(a-f) show that ozone and atomic oxygen abundances are strongly influenced by HO_y and Cl_y in the upper stratosphere, where the HO_2+O and ClO+O cycles maximize. At 1 hPa, the increase in HO_y leads to ∼8% less O by 2090 (Figure 3.3(a), grey line minus dashed black line) such that less O is available to participate in Cycle I. Because CH_4 is a source of reactive hydrogen, the effectiveness of N_2O as an ODS is weakened by elevated CH_4 concentrations. The effect of Cl_y on odd-oxygen at 2 hPa is largest in 1990, when there is a 14% decrease in O (Figure 3.3(b), red line minus dashed black line). Cl_y becomes less important for ozone depletion through the 21st century as its concentration decreases.

Long-term cooling of the stratosphere decreases the O/O_3 ratio (Figures 3.3(g-i)) and leads to ∼20% more ozone by 2090 in the upper stratosphere at 1 and 2 hPa (Figures 3.3(d-e), dashed black line minus blue line). Because the O/O_3 ratio decreases with stratospheric cooling, less atomic oxygen is available for Cycle I for a constant O_3 mixing ratio. Partitioning between O

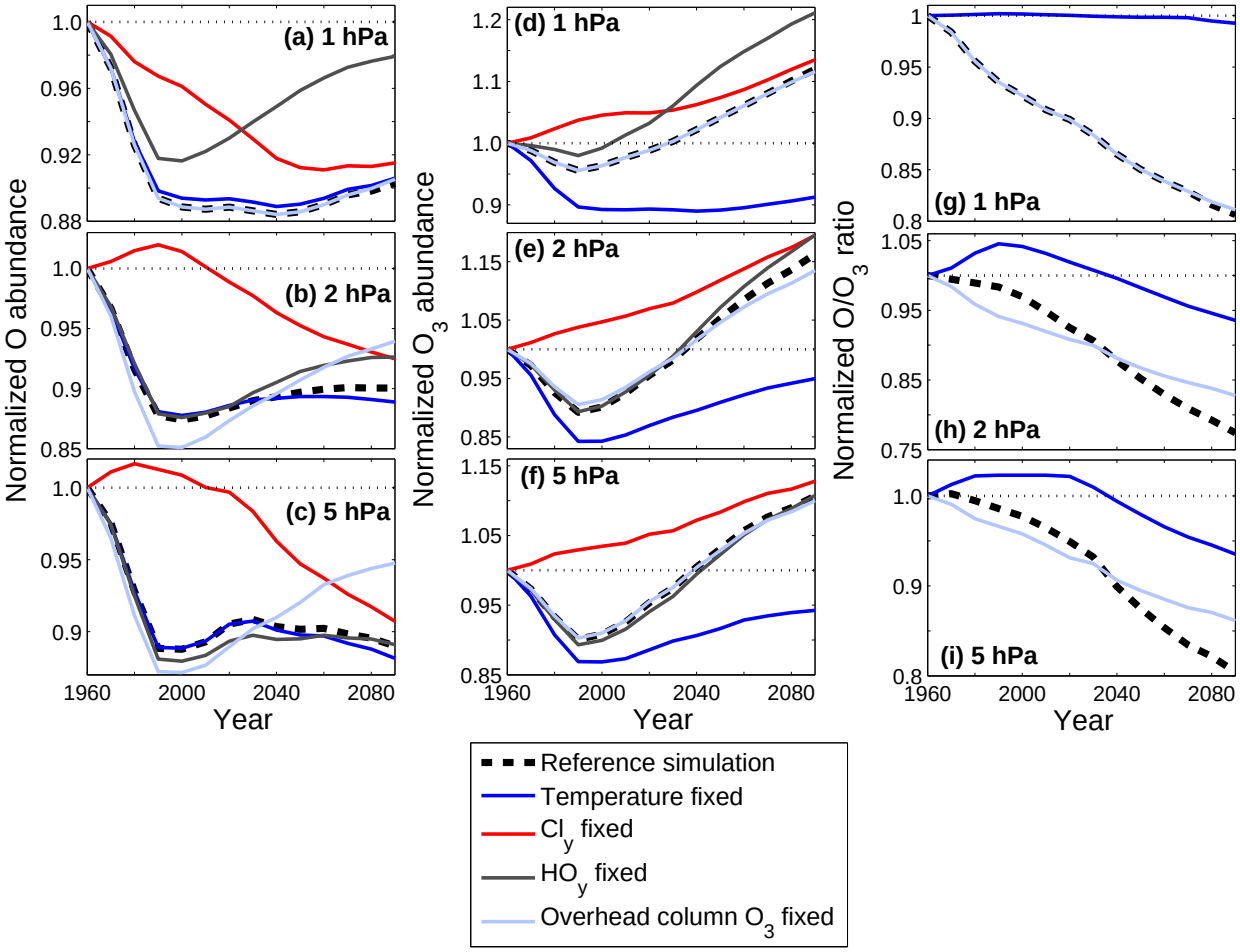

Figure 3.3: *Box model simulations at 2°N showing normalised (to 1960) local atomic oxygen abundances (a-c), ozone abundances (d-f), and the O/O_3 ratio (g-i) at 1, 2 and 5 hPa. The reference simulation allowed all parameters to evolve, whilst the other four simulations kept one of temperature, Cl_y, HO_y and overhead column ozone fixed (all other parameters were allowed to evolve). The Cl_y and HO_y curves are omitted in (g-i) because they display no effect on O/O_3.*

and O_3 is also influenced by overhead column ozone at 2 and 5 hPa (Figures 3.3(h-i)), which modulates the local flux of UV radiation.

3.4 Conclusions

Ravishankara et al. [2009] estimated the effects of increasing emissions of N_2O on ozone assuming constant stratospheric GHG concentrations. Here, a complementary, but different, question is addressed: How, and to what extent, might various mechanisms associated with the stratospheric cooling effects of GHG increases (which are scenario dependent) mitigate the effects of N_2O on ozone? The results presented here indicate that while N_2O is an important gas for ozone depletion through the 21st century (in accordance with the findings of *Ravishankara*

et al. [2009]), a number of factors mitigate its effectiveness in depleting ozone. CO_2-induced stratospheric cooling and the strengthening of the Brewer-Dobson circulation decrease the yield of NO_x from N_2O by decreasing the NO_y/N_2O, NO_x/NO_y and NO_2/NO ratios. In addition, it is shown that changes in the hydrogen and chlorine chemical cycles, whose rates are modulated by changes in emissions of CH_4 and chlorine-containing compounds, moderate the effectiveness of the NO_2+O cycle (the dominant NO_x cycle) by catalytically depleting odd-oxygen, thereby reducing the availability of atomic oxygen for the NO_2+O reaction.

Chapter 4

Impacts of the production and consumption of biofuels on stratospheric ozone

The work presented in Chapter 3 implies that a future in which CO_2 emissions decrease (leading to reduced stratospheric cooling), and N_2O emissions increase, could be detrimental to stratospheric ozone through the expected enhancement in NO_x-induced ozone destruction. Such a future could occur under a large-scale shift from fossil fuels to biofuels production and consumption; reducing fossil fuel consumption would decrease CO_2 emissions, and growing crops for biofuels would incur a large increase in N_2O emissions resulting from the application of nitrogen-based fertilizers. Here, the potential effects on the ozone layer of a large-scale shift away from fossil fuel use to biofuels consumption over the 21^{st} century are examined. Three CCM simulations were performed, designed to quantify the effects on stratospheric ozone of reduced stratospheric cooling and increased N_2O emissions.

4.1 Introduction

As fossil fuel reserves diminish and awareness of the detrimental effects of fossil fuel burning on global climate continues to grow, biofuels are becoming an increasingly attractive supply of fuel, especially in Europe, the USA and Brazil [*Bessou et al.*, 2011]. In 2010, biofuels accounted for 2.7% of road-transportation fuel use globally (http://vitalsigns.worldwatch.org/vs-trend/biofuels-regain-momentum). They are often considered to be carbon neutral because the CO_2 released on burning had previously been removed from the atmosphere via photosynthesis. However, nitrogen-based fertilizers used in growing the crops from which biofuels are produced lead to N_2O emissions via soil nitrification and denitrification [*Smeets et al.*, 2009].

N_2O is a GHG with a 100-year GWP of ∼298, and a lifetime of ∼114 years [*Forster et al.*, 2007]. *Crutzen et al.* [2008] suggested that the global warming mitigation achieved through CO_2 reductions by using first-generation biofuels (those produced from vegetable oil, starch or sugar) instead of fossil fuels, could be countered by the subsequent increase in N_2O emissions resulting from increased nitrogen-based fertilizer use.

Using linked economic and terrestrial biogeochemistry models, *Melillo et al.* [2009] studied changes in CO_2 emissions due to fossil fuel abatement and land-use changes, and fertilizer N_2O emissions under two possible scenarios for a global biofuels programme: one in which existing managed land is used more intensely; the other allowing the conversion of natural areas to managed land, as long as it is profitable to do so. They found that CO_2 emissions from land-use changes, although significant, would be less than the CO_2 "saved" from fossil fuel abatement by the end of the 21st century. However, an increase in N_2O emissions due to increases in nitrogen-based fertilizer use would be an important contributor to climate warming, and under both scenarios would account for ∼60% of total annual N_2O emissions by 2100.

As well as being a GHG, N_2O leads to stratospheric ozone destruction through its reaction with $O(^1D)$ to produce NO_x (for further details see Section 1.3.1). The effectiveness of N_2O in depleting stratospheric ozone is mitigated by CO_2-induced stratospheric cooling, as discussed in Section 3.1.

Three CCM simulations denoted 'A1B', 'B1' and 'biofuels' (Table 4.1) were performed to examine the potential effects of increased production and consumption of biofuels on stratospheric ozone.

Table 4.1: *Summary of the three CCM simulations*

	A1B	B1	Biofuels
N_2O emissions in 2100 (MtN_2O-N)[a]	7.0	5.7	14.3
CO_2 emissions in 2100 (GtC)	13.1	5.2	3.7
2090s temperature (K)[b]	215.2	218.6	218.9
ΔO_3 (DU)[c]	9.1	-0.7	-2.6

[a] *MtN_2O-N refers to the Mt of N in N_2O.*
[b] *Global-mean temperatures at 30 hPa simulated by NIWA-SOCOL, and averaged over the 2090s decade.*
[c] *Change in global-mean total column ozone over the 21^{st} century simulated by NIWA-SOCOL (2090s decade minus 2010s decade).*

The A1B and B1 simulations were based on the IPCC SRES A1B and SRES B1 GHG emissions scenarios, respectively (Section 2.4). The A1B and B1 simulations display similar N_2O surface concentrations but different CO_2 surface concentrations and different SSTs, which influence stratospheric temperatures and the Brewer-Dobson circulation respectively. This facilitated an investigation of how the Brewer-Dobson circulation and CO_2-induced stratospheric cooling influence ozone and ozone-depleting NO_x chemistry. The major difference between the B1 and biofuels simulations was the N_2O surface concentrations, permitting a study of the effect of increased N_2O emissions on ozone as a result of increased nitrogen-based fertilizer use.

4.2 Emissions scenarios

The MAGICC6 SCM [*Meinshausen et al.*, 2011a] was used to convert emissions scenarios to the surface concentration scenarios required as input to the CCM simulations. CCM simulations were performed from 2000-2100 using the NIWA-SOCOL model, with the first ten years treated as spin-up. The reaction rate constants used were those recommended by *Sander et al.* [2006, 2009]. See Chapter 2 for further details of the MAGICC6 and NIWA-SOCOL models.

For the B1 simulation, surface concentrations of CO_2, N_2O and CH_4, commensurate with the SRES B1 emissions scenario, were calculated using MAGICC6. SSTs and SICs were prescribed using output from the United Kingdom Met Office – Hadley Centre Coupled Model v.3 (UKMO-HadCM3) AOGCM, based on the SRES B1 emissions scenario [*Nakicenovic and Swart*, 2001]. The SST and SIC datasets were obtained from the World Climate Research Programme's CMIP3 multimodel dataset.

Since the biofuels simulation was constructed to follow the same radiative forcing pathway as the B1 simulation (see below), it used the same SSTs, SICs and CH_4 surface concentrations as the B1 simulation. The biofuels simulation was based on findings from *Melillo et al.* [2009], which suggest that biofuels production and the associated use of nitrogen-based fertilizers could account for ∼60% of total annual N_2O emissions by 2100. To capture this effect, an emissions scenario for N_2O, with emissions of 14.3 MtN_2O-N in 2100 compared with 5.7 MtN_2O-N in the B1 scenario, was constructed. MAGICC6 calculated the corresponding surface N_2O concentrations, which were 443 ppb in 2100 compared with 368 ppb in the B1 scenario (Figure 4.1(a)).

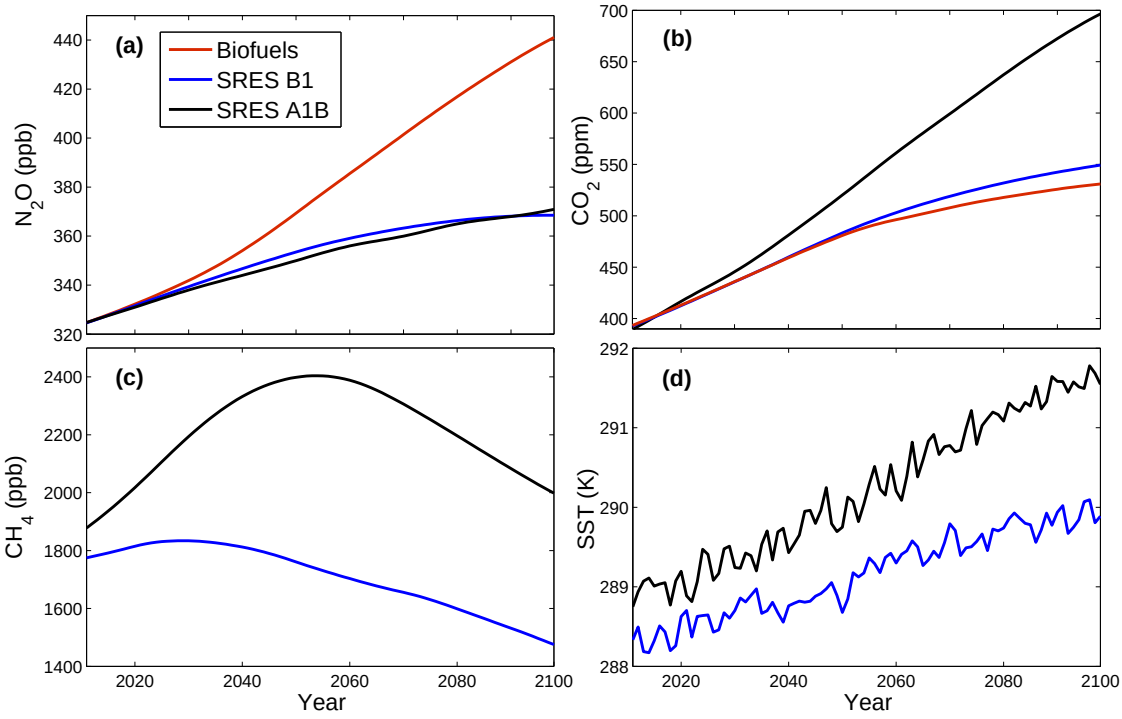

Figure 4.1: *(a) N_2O, (b) CO_2, (c) CH_4 surface concentrations for the A1B, B1 and biofuels emissions scenarios (the biofuels simulation used B1 CH_4 concentrations). (d) Global-mean SSTs for the A1B and B1 simulations (the biofuels simulation used B1 SSTs).*

CO_2 emissions used in the biofuels scenario were slightly lower than those prescribed in the B1 scenario in order to make the global-mean radiative forcing in the biofuels simulation the same as that in the B1 simulation. By keeping the radiative forcings the same, it was ensured that any differences between the simulations were attributable to changes in chemistry and were not potentially compromised by changes in dynamics. The reduction in CO_2 concentrations also served to simulate the expected reduction in CO_2 emissions resulting from use of biofuels rather than fossil fuels. This resulted in CO_2 emissions of 3.7 GtC in 2100 in the biofuels scenario, compared with 5.2 GtC in the B1 scenario (Table 4.1). The equivalent CO_2 surface concentrations in 2100, calculated using MAGICC6, were 532 ppm in the biofuels scenario,

compared with 551 ppm in the B1 scenario (Figure 4.1(b)).

The A1B simulation used GHG concentrations, SSTs and SICs consistent with the SRES A1B scenario. SSTs and SICs were taken from ECHAM5/MPIOM AOGCM output. SSTs for the A1B and B1 simulations are shown in Figure 4.1(d). CH_4 concentrations are displayed in Figure 4.1(c) (note that the biofuels simulation used B1 SSTs).

4.3 Results and discussion

The projected changes in global-mean total column ozone over the 21st century for the three simulations are summarized in Table 4.1. In the A1B simulation, global-mean total column ozone is projected to increase by 9.1 DU through the 21st century, due to a slowing of the halogen ozone-loss cycles and CO_2-induced stratospheric cooling (Section 1.2.3). This result is consistent with other CCM projections presented and discussed in the SPARC CCMVal-2 assessment, which also used the SRES A1B scenario [*Eyring et al.*, 2010a].

In the B1 simulation, column ozone decreases by 0.7 DU over the 21st century since stratospheric cooling is less than in the A1B simulation. A larger decrease in column ozone of 2.6 DU is calculated in the biofuels simulation, because greater N_2O emissions in that case also lead to enhanced rates of the ozone-depleting NO_x cycles.

Ozone differences between the B1 and A1B simulations at the end of the 21st century are displayed in Figure 4.2(a) as a percentage of ozone in the A1B simulation, and in Figure 4.2(b) as the difference in total column ozone (B1 minus A1B). These plots facilitate an assessment of the effect of GHG forcing (for example, driving changes in stratospheric temperatures and the Brewer-Dobson circulation) on ozone. The ozone concentrations in the B1 simulation in the upper and lower Antarctic stratosphere and the tropical lower stratosphere (red regions of Figure 4.2(a)) are greater than those in the A1B simulation, consistent with the findings of *Eyring et al.* [2010b]. Elsewhere, the B1 simulation ozone concentrations are generally lower by as much as 20%.

The regions of lower ozone concentrations in the B1 simulation (blue areas of Figure 4.2(a)) are likely due to: 1) the weaker stratospheric cooling, with the result that the temperature-dependent gas-phase ozone-loss cycles slow less than in the A1B simulation; 2) lower CH_4 concentrations than in the A1B scenario (CH_4 increases the ozone column, as discussed in Chapter 5) and; 3) reduced strengthening of the Brewer-Dobson circulation, as a result of cooler SSTs [*Fomichev*

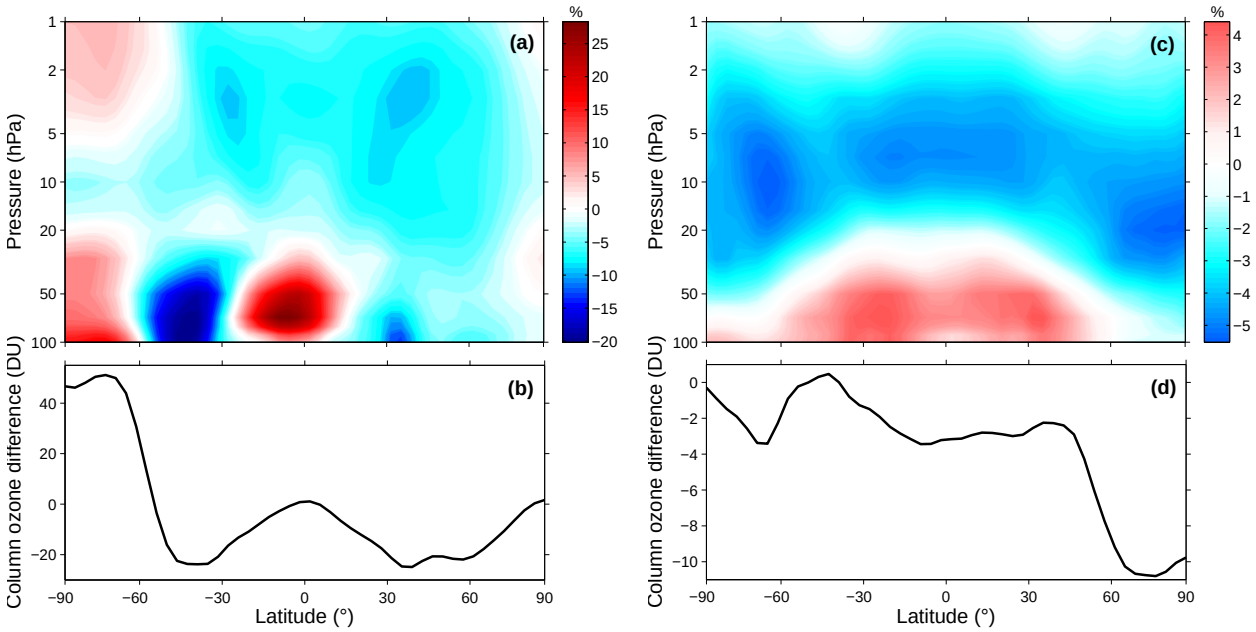

Figure 4.2: *(a) B1 ozone minus A1B ozone in the 2090s decade, calculated as a percentage of ozone in the A1B simulation. (b) 2090s decade B1 total column ozone minus A1B total column ozone. (c) Biofuels ozone minus B1 ozone in the 2090s decade, calculated as a percentage of ozone in the B1 simulation. (d) 2090s decade biofuels total column ozone minus B1 total column ozone.*

et al., 2007; *Bekki et al.*, 2011], which means that the ozone flux into the southern mid-latitude lower stratosphere is weaker than in the A1B simulation.

Increased tropical lower-stratospheric ozone in the B1 simulation is consistent with a difference in the Brewer-Dobson circulation between the B1 and A1B simulations. The slower ascent rate in the tropical lower stratosphere in the B1 simulation allows more time for ozone to form in the rising air parcels than in the more quickly ascending air in the A1B simulation [*Avallone and Prather*, 1996]. Elevated lower-stratospheric Antarctic ozone in the B1 simulation is caused by a relatively warmer lower stratosphere; over the 21st century, Antarctic winter temperatures at 50 hPa average 197 K in the B1 simulation compared to 189 K in the A1B simulation. As a result, PSC formation, and the associated heterogeneous chlorine and bromine ozone-depleting chemistry, is suppressed in the B1 simulation compared to the A1B simulation. In contrast, the Arctic does not get as cold as the Antarctic during winter (Section 1.2.2), so a similar increase in ozone is not observed there. In the 2090s, there is ∼5% more upper-stratospheric Antarctic ozone in the B1 simulation than in the A1B simulation because there is less CH_4, and hence the ozone-depleting HO_x cycles (which are dominant in the upper stratosphere) are slower.

Figures 4.2(c) and (d) display the same difference quantities as Figures 4.2(a) and (b), but calculated between the biofuels and B1 simulations. These facilitate an assessment of the effects of larger N_2O emissions on ozone. Figure 4.2(c) shows that, under the biofuels scenario, ozone concentrations are (relatively) suppressed throughout the middle stratosphere and enhanced in the lower stratosphere, especially at mid- and equatorial latitudes. However, because the middle stratosphere dominates the ozone column, total column amounts are smaller in the biofuels simulation and up to 11 DU less at northern high latitudes (Figure 4.2(d)).

In the biofuels simulation, ozone is greater by up to 4% in the troposphere and lower stratosphere compared to that in the B1 simulation. N_2O leads to an increase in tropospheric ozone production, via Reaction-cycle 4.1:

$$\begin{aligned} \mathrm{OH + CO} &\longrightarrow \mathrm{H + CO_2} \\ \mathrm{H + O_2 + M} &\longrightarrow \mathrm{HO_2 + M} \\ \mathrm{HO_2 + NO} &\longrightarrow \mathrm{NO_2 + OH} \\ \mathrm{NO_2 + h\nu} &\longrightarrow \mathrm{NO + O} \\ \mathrm{O + O_2 + M} &\longrightarrow \mathrm{O_3 + M} \\ \hline \mathrm{CO + 2O_2} &\longrightarrow \mathrm{CO_2 + O_3} \end{aligned} \tag{4.1}$$

Ozone production by this mechanism is generally insignificant in the stratosphere, where the concentration of CO is too small [*Lanzendorf et al.*, 2001].

In the middle and upper stratosphere, ozone in the biofuels scenario is up to 5% less than that in the B1 simulation, since N_2O concentrations are higher, leading to a faster rate of the ozone-depleting NO_x cycles (Cycles I and II – see Appendix A). These cycles do not occur in the troposphere where O and O_3 concentrations are small.

Figure 4.3 shows the combined rate of the two NO_x ozone-loss cycles (Cycles I and II), averaged over 1-100 hPa, relative to their rate in 2010 for each of the three simulations. Despite increasing N_2O emissions in the A1B simulation, NO_x-induced ozone depletion slows over the 21st century, as described in Chapter 3 and *Revell et al.* [2012]. The B1 simulation has N_2O emissions almost identical to those in the A1B simulation, yet, because the stratosphere cools relatively less, the rate at which the NO_x cycles deplete ozone increases by ∼2% between 2010 and 2100. Finally, in the biofuels simulation, the rate of ozone-depleting NO_x chemistry increases by ∼10% over the 21st century owing to the large increase in N_2O concentrations.

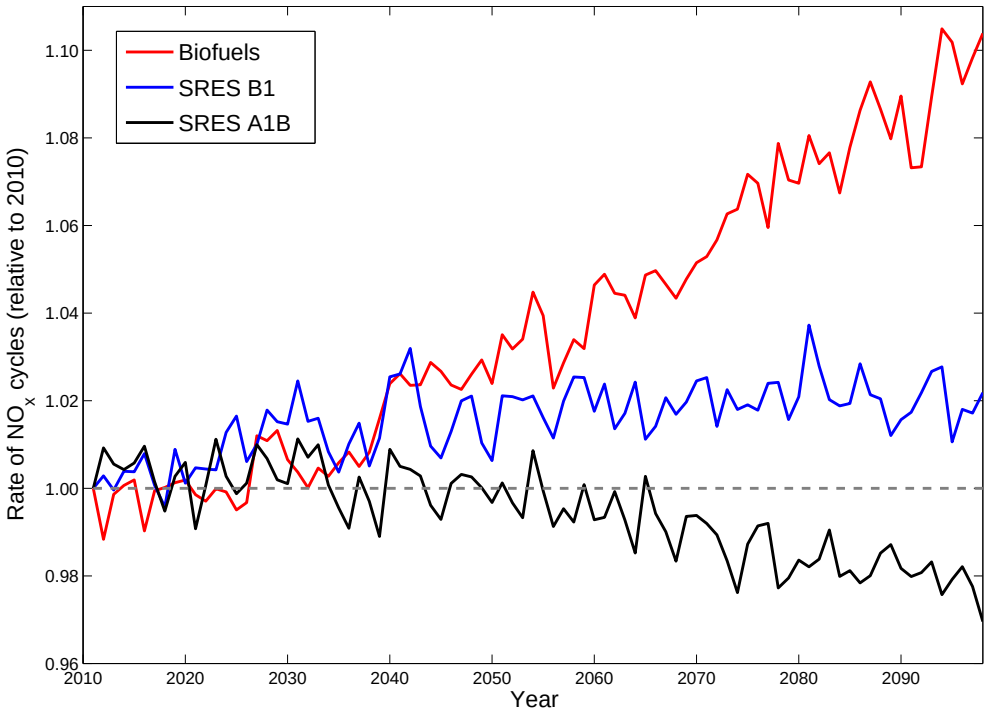

Figure 4.3: *Global-mean rate of the NO_x ozone-loss cycles, averaged over 1-100 hPa and normalised to 1.0 in 2010. The differences between the biofuels and B1 simulations are largely a consequence of different N_2O emissions, while those between the B1 and A1B simulations are largely due to temperature differences.*

4.4 Conclusions

The effects of three different GHG emissions scenarios on stratospheric ozone have been examined. The SRES A1B scenario is the scenario on which the majority of the SPARC CCMVal-2 simulations were based. In the A1B simulation, global-mean total column ozone increases by 9.1 DU over the 21st century due to decreasing halogen concentrations and GHG-induced stratospheric cooling. Such an increase was not observed in the simulation based on the SRES B1 scenario (0.7 DU decrease), which has lower CO_2 and CH_4 emissions. Increasing N_2O emissions increase the rate of NO_x-catalysed ozone loss, and this effect becomes more pronounced when the stratosphere cools relatively less, as it does in the biofuels simulation (2.6 DU decrease). Therefore, the reduction in CO_2 emissions achieved by switching to biofuels is not large enough to compensate for the deleterious effects of associated increases in N_2O emissions on stratospheric ozone.

Use of biofuels to ameliorate global climate change has many problems, such as diverting crops from food, clearance of forests for agriculture, and the inefficiency of crop to fuel conversion. Added to this, the work presented in this chapter shows that the increase in N_2O emissions

resulting from increased biofuels production and consumption could damage the ozone layer.

Chapter 5

The sensitivity of stratospheric ozone changes through the 21st century to N_2O and CH_4

Anthropogenic emissions of the GHGs N_2O and CH_4 are projected to increase through the 21^{st} century, leading to increases in their atmospheric concentrations. Consequently, NO_x and HO_x species produced from N_2O and CH_4, respectively, are expected to play an increasingly important role in determining stratospheric ozone concentrations. Although the roles of N_2O and CH_4 in ozone chemistry are qualitatively understood, the sensitivity of ozone to these gases has not been thoroughly investigated. To gain a quantitative understanding of the sensitivity of stratospheric ozone to N_2O and CH_4, eight CCM simulations were performed; four each to assess the sensitivity of ozone to N_2O and CH_4 changes. Because CO_2 is the main driver of 21^{st} century stratospheric dynamical changes, the same CO_2 scenario was used across all eight CCM simulations. These simulations were used to investigate the chemical effects of CH_4 and N_2O on stratospheric composition.

5.1 Introduction

Through the 21st century, declining concentrations of stratospheric chlorine and bromine, together with increasing concentrations of CO_2, are projected to lead to increased global-mean stratospheric ozone (Section 1.2.3). Of the GHGs controlled under the Kyoto Protocol, those with the highest radiative forcings after CO_2 are N_2O and CH_4, both of which lead to changes in ozone via chemical processes (Section 1.3).

N_2O in the stratosphere affects ozone predominantly through NO_x-catalysed ozone-loss cycles. However, as concluded in Chapter 3, increases in N_2O do not necessarily lead to increases in NO_x-catalysed ozone depletion, due to the interfering effects of other GHGs and ODSs.

The oxidation of CH_4 produces HO_x radicals (Reaction 1.18), which catalyse ozone destruction cycles such as Cycles IV-VIII in Appendix A. These cycles are particularly important in the upper stratosphere, where HO_x abundances are large (see Figure 3.2(b)). However, *Portmann and Solomon* [2007] and *Fleming et al.* [2011] have shown that the predominant effect of increasing CH_4 is to increase total column ozone by way of H_2O-induced cooling in the middle stratosphere, which slows the temperature dependent gas-phase ozone-loss cycles (Section 1.3.2). In addition, increasing CH_4 increases the rate of Reaction 5.1 (see below), which increases the rate of conversion of chlorine to the HCl reservoir and thereby slows the chlorine-catalysed ozone-loss cycles throughout the stratosphere.

$$CH_4 + Cl \longrightarrow CH_3 + HCl \tag{5.1}$$

Furthermore, in the troposphere and lowermost stratosphere, where the concentration of CO is sufficiently large [*Lanzendorf et al.*, 2001], increases in both HO_x and NO_x cause an increase in the rate of Reaction-cycle 4.1, thereby leading to ozone production [*Brasseur and Solomon*, 2005; *Fleming et al.*, 2011].

Oman et al. [2010] studied the effects of NO_x and HO_x on stratospheric ozone using two CCM simulations constrained by the IPCC SRES A1B and A2 emissions scenarios for GHGs, which portray intermediate (A1B) and large (A2) increases in CO_2, N_2O and CH_4 through the 21st century [*Nakicenovic and Swart*, 2001]. The evolution of upper-stratospheric ozone in the two simulations was similar because, although NO_x and HO_x species led to larger ozone losses in A2 compared with A1B, they were compensated by the effects of larger increases in CO_2-induced stratospheric cooling, which slowed ozone loss rates.

Here, an analysis of the chemical sensitivity of stratospheric ozone to N_2O and CH_4 through the 21st century is presented using the results from eight CCM simulations. The inputs of four simulations differed only in terms of their N_2O concentrations, while the other four differed only by their CH_4 concentrations. The same concentration scenario for CO_2 was used across all eight simulations.

5.2 Concentrations scenarios

Eight GHG concentration scenarios were constructed, as described in Table 5.1, using combinations of the IPCC SRES A1B concentrations scenarios for GHGs and the four RCPs (see Section 2.4). Surface concentrations of N_2O and CH_4 for the individual scenarios are shown in Figure 5.1. All simulations used the SRES A1B scenario for CO_2 and the adjusted A1 scenario for halocarbons (Section 2.4).

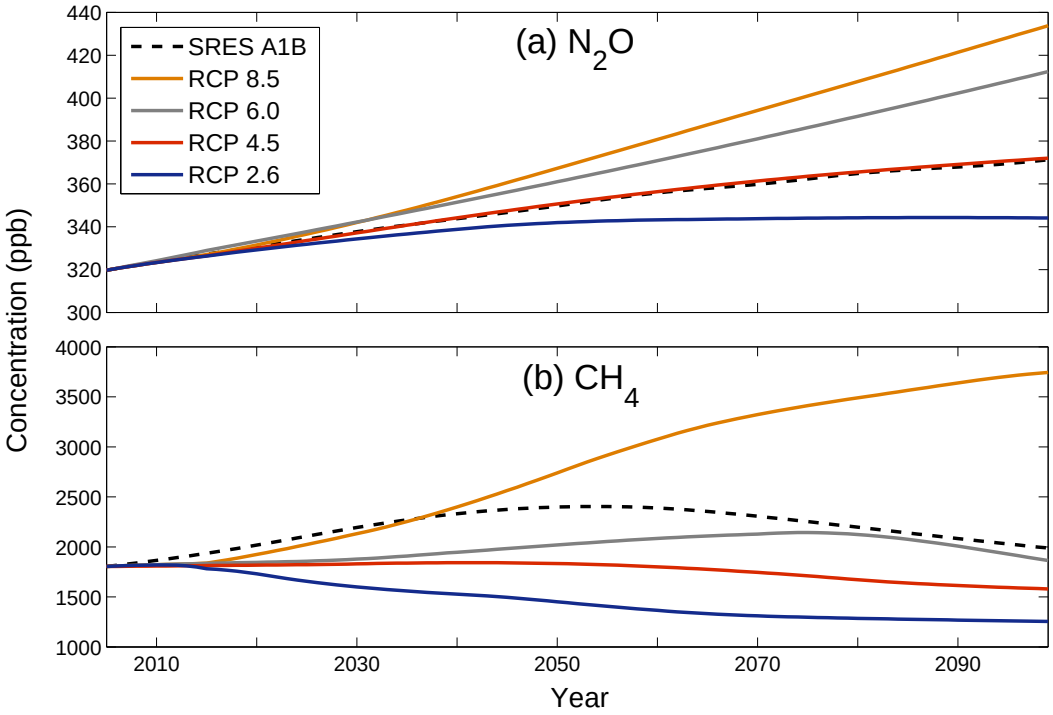

Figure 5.1: *(a) N_2O and (b) CH_4 surface concentrations used in the CCM simulations.*

SSTs were prescribed under the SRES A1B scenario using output from the ECHAM5/ MPIOM AOGCM. To test whether the SSTs would have been different if they had been calculated from AOGCM simulations using the constructed GHG concentration scenarios (Table 5.1), SSTs for each of the eight scenarios were simulated using the MAGICC6 SCM (Section 2.2). Globally averaged annual-mean SSTs under the eight GHG concentrations scenarios as well as

Table 5.1: *Summary of CCM simulations*

Simulation[a]	N_2O scenario	CH_4 scenario	ΔO_3 (DU)[b]
N_2O-2.6	RCP 2.6	SRES A1B	10.0
N_2O-4.5	RCP 4.5	SRES A1B	7.6
N_2O-6.0	RCP 6.0	SRES A1B	4.9
N_2O-8.5	RCP 8.5	SRES A1B	4.3
CH_4-2.6	SRES A1B	RCP 2.6	4.4
CH_4-4.5	SRES A1B	RCP 4.5	5.2
CH_4-6.0	SRES A1B	RCP 6.0	9.1
CH_4-8.5	SRES A1B	RCP 8.5	16.7

[a] *All simulations used the IPCC SRES A1B scenario for CO_2 and adjusted A1 scenario for halocarbons.*
[b] *Change in global-mean total column ozone through the 21^{st} century (2090s decade minus the decade from 2015-2024).*

the SRES A1B scenario are displayed in Figure 5.2. SSTs exhibit a greater spread by 2100 in simulations employing different CH_4 scenarios, owing to the greater radiative forcing of CH_4 (0.48 W m^{-2}) compared with N_2O (0.16 W m^{-2}) [*Forster et al.*, 2007]. However, the results are sufficiently similar to the SRES A1B simulation (at most, there is a difference of 0.5 K in global-mean SSTs between the CH_4-8.5- and SRES A1B-based SSTs in 2100) that the conclusions drawn in this study are not invalidated by using SRES A1B-based SSTs for all simulations.

The eight NIWA-SOCOL CCM simulations, each using one of the concentration scenarios described in Table 5.1, were run from 2005-2100, with the first ten years treated as spin-up.

5.3 Results and discussion

In all eight CCM simulations, global-mean total column ozone increases through the 21^{st} century, by the amounts listed as ΔO_3 in the rightmost column of Table 5.1. In general, this increase is caused by a combination of a slowing of the gas-phase ozone-loss cycles due to stratospheric cooling [*Rosenfield et al.*, 2002], and decreasing concentrations of stratospheric chlorine and bromine resulting from the phase-out of halogenated ODSs under the Montreal Protocol [*Bekki et al.*, 2011]. The simulations with larger N_2O surface concentrations lead to smaller increases in ozone (4.3 DU in N_2O-8.5 compared with 10 DU in N_2O-2.6), while those with larger CH_4 surface concentrations lead to a larger increase in ozone (16.7 DU in CH_4-8.5

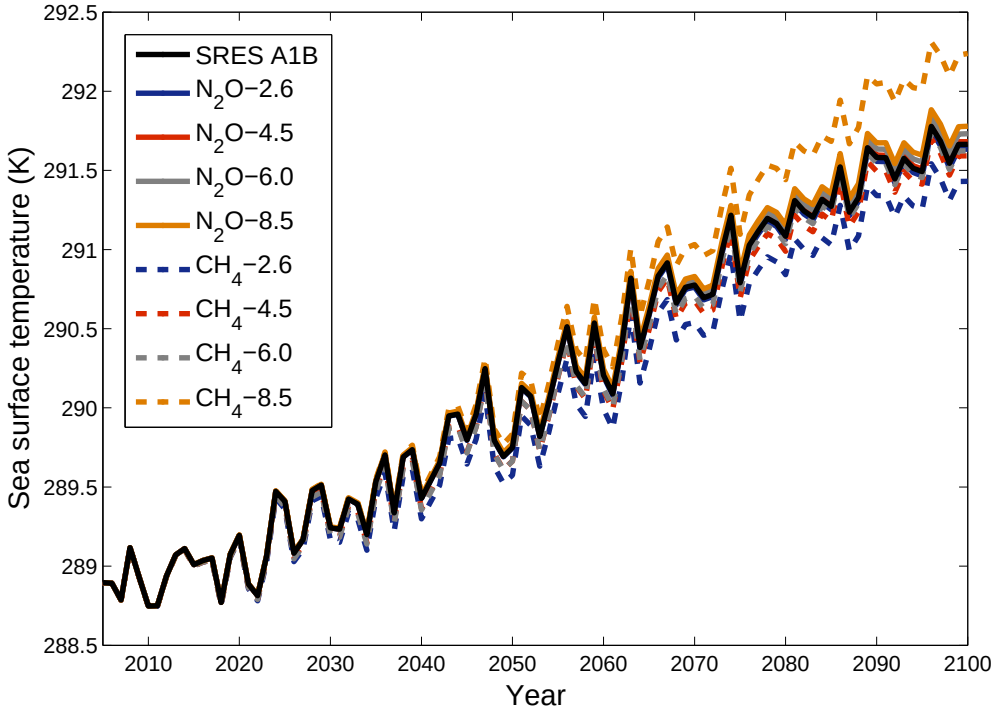

Figure 5.2: *Global-, annual-mean SSTs. The SRES A1B SSTs were used in all eight CCM simulations. The other SST series were calculated individually for each GHG concentration scenario using MAGICC6.*

compared with 4.4 DU in CH_4-2.6).

To examine changes in chemically induced ozone destruction, the differences in the global-mean rates of the nitrogen, hydrogen and chlorine cycles in the 2090s decade between (a) the N_2O-8.5 and N_2O-2.6 simulations and (b) the CH_4-8.5 and CH_4-2.6 simulations are shown in Figure 5.3. The ozone-depleting nitrogen cycles strengthen with increased N_2O throughout the upper and middle stratosphere, but remain largely unchanged in the lower stratosphere where concentrations of odd oxygen are diminished (Figure 5.3(a)). Figure 5.3(b) shows that the ozone-depleting hydrogen cycles speed up with increased CH_4, particularly in the upper stratosphere. The chlorine cycles slow quite substantially, due to the increasing rate of Reaction 5.1 which converts active chlorine (Cl) to the chlorine reservoir HCl.

Figure 5.4(a) shows the difference between 2090s-ozone in the N_2O-8.5 and N_2O-2.6 simulations as a function of latitude and pressure. Ozone is suppressed by as much as ∼5-10% in the middle stratosphere in the N_2O-8.5 simulation compared to the N_2O-2.6 simulation but is elevated by ∼5% in the tropical lower stratosphere (∼100-70 hPa). The smaller ozone increase in the N_2O-8.5 simulation is expected and is due to enhanced rates of the ozone-depleting nitrogen cycles. The elevated values in the tropical lower stratosphere are due to ozone production

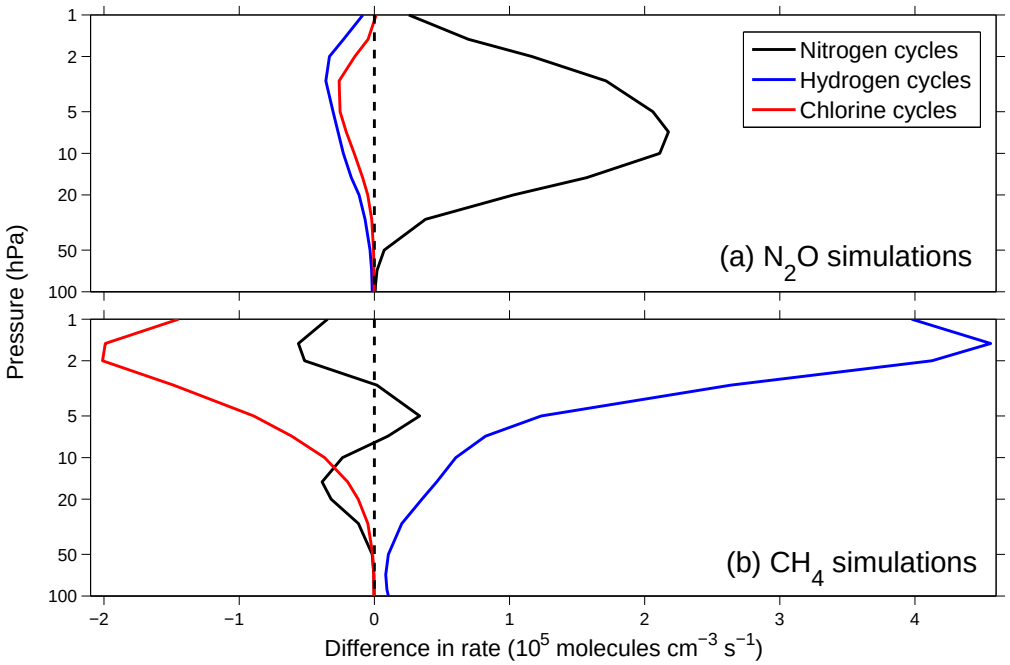

Figure 5.3: *(a) Global-mean contribution to ozone loss from the nitrogen, hydrogen and chlorine catalytic cycles in the 2090s decade in the N_2O-8.5 simulation, minus the same quantities for the N_2O-2.6 simulation. (b) Global-mean contribution to ozone loss from catalytic cycles in the 2090s decade in the CH_4-8.5 simulation, minus the same quantities for the CH_4-2.6 simulation.*

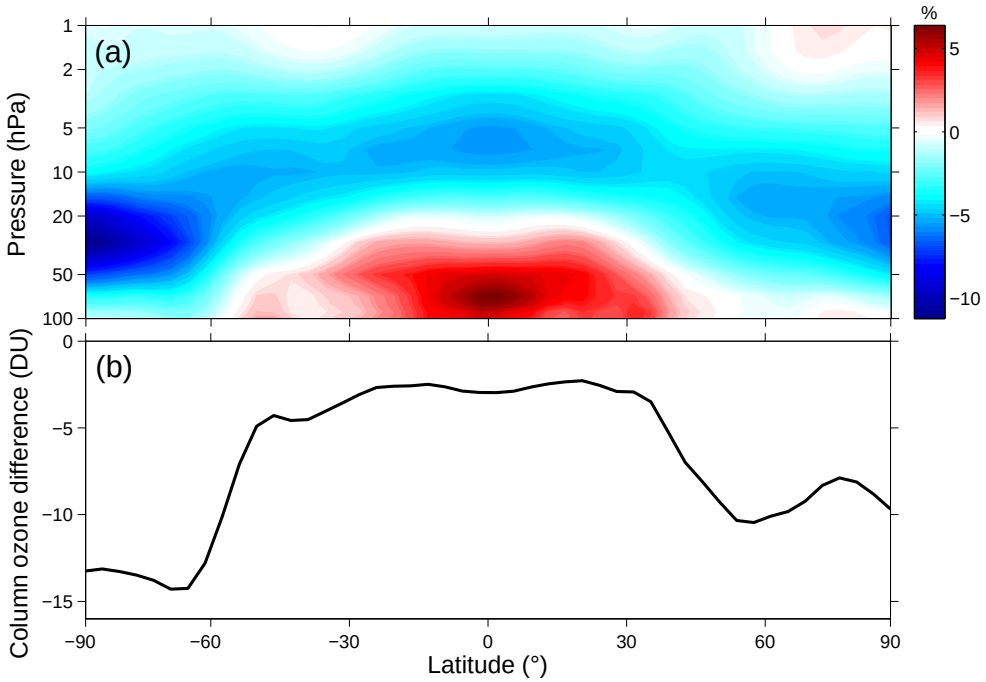

Figure 5.4: *(a) N_2O-8.5 ozone minus N_2O-2.6 ozone in the 2090s decade, calculated as a percentage of ozone in the N_2O-2.6 simulation. (b) 2090s-decade N_2O-8.5 total column ozone minus N_2O-2.6 total column ozone.*

via Reaction-cycle 4.1. The difference between 2090s total column ozone in the N_2O-8.5 and N_2O-2.6 simulations is shown in Figure 5.4(b) as a function of latitude. Because the middle stratosphere dominates the ozone column, total column ozone is smaller at all latitudes in the N_2O-8.5 simulation relative to the N_2O-2.6 simulation (more so at polar latitudes).

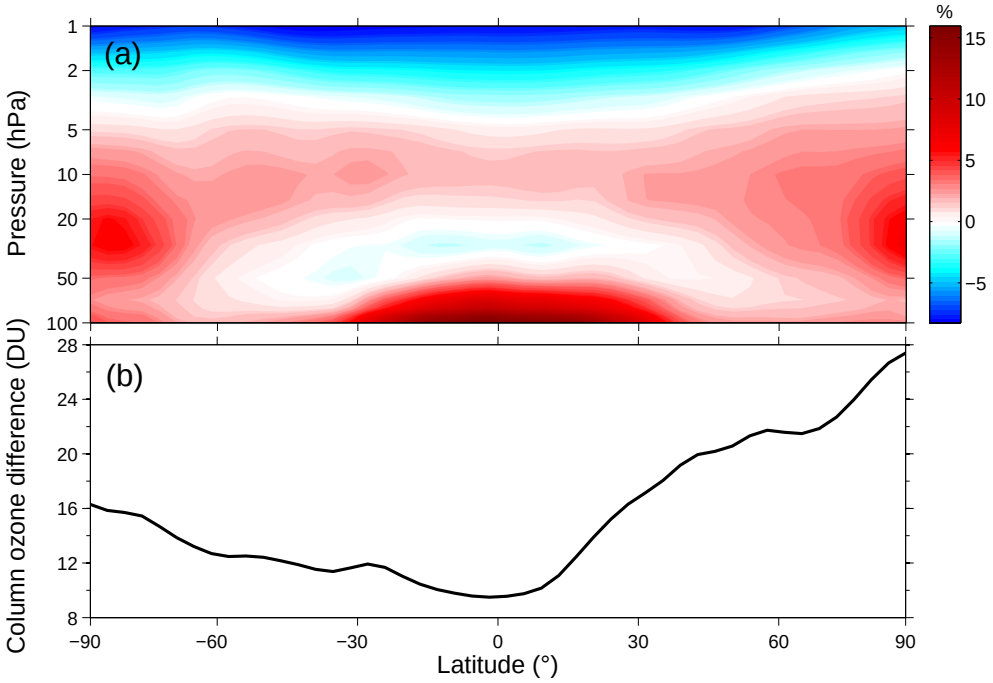

Figure 5.5: *(a) CH_4-8.5 ozone minus CH_4-2.6 ozone in the 2090s decade, calculated as a percentage of ozone in the CH_4-2.6 simulation. (b) 2090s-decade CH_4-8.5 total column ozone minus CH_4-2.6 total column ozone.*

Figure 5.5 is similar to Figure 5.4, but shows the differences between simulations CH_4-8.5 and CH_4-2.6. In simulation CH_4-8.5, ozone increases up to ∼15% greater than those in the CH_4-2.6 simulation are seen throughout the stratosphere, except for in the upper stratosphere where ozone is suppressed by more than 5% due to enhanced rates of the HO_x ozone-loss cycles. The general increase in ozone in the middle and lower stratosphere can be attributed to an increase in the rate of Reaction 5.1 (slowing the chlorine ozone-loss cycles); an increase in the rate of Reaction-cycle 4.1 due to increased HO_x in the lower stratosphere (leading to increased ozone production); a slowing of the nitrogen ozone-loss cycles at ∼15 hPa (Figure 5.3(b)), and a small contribution to stratospheric cooling resulting from increased water vapor. Figure 5.5(b) shows that 2090s total column ozone exhibits a larger increase at all latitudes in simulation CH_4-8.5 compared with simulation CH_4-2.6, and particularly in the Arctic.

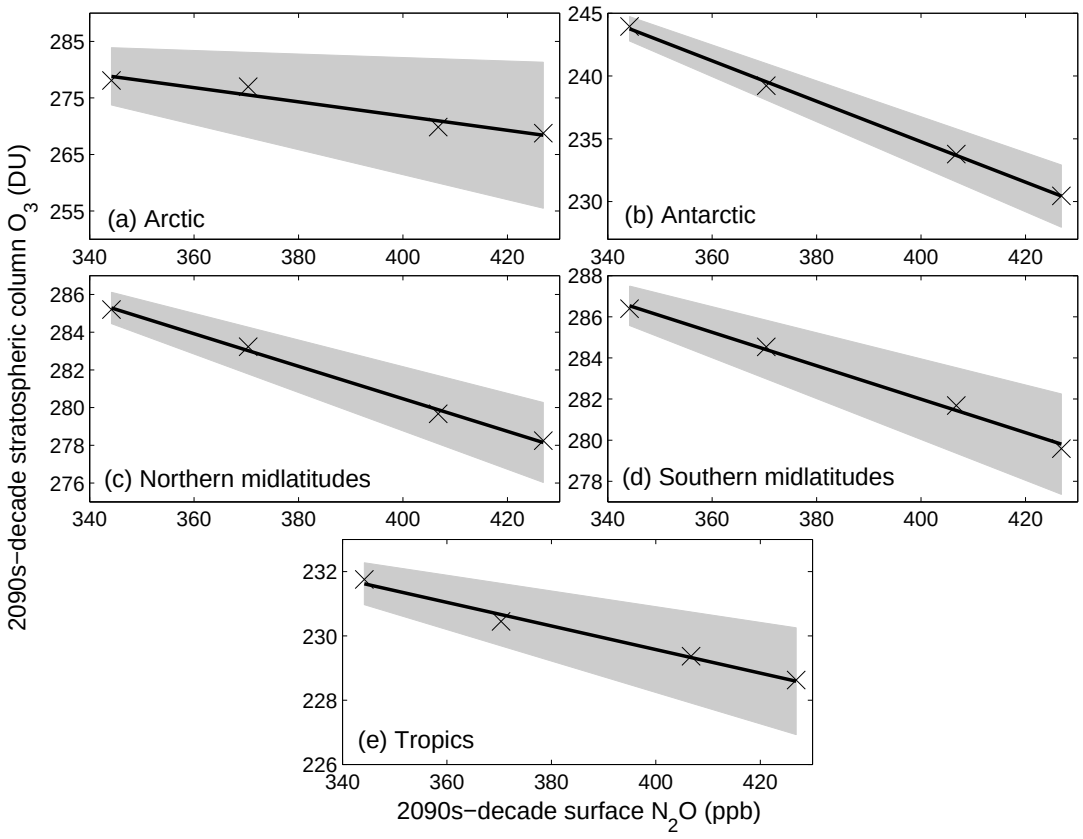

Figure 5.6: *(a) 2090s-mean Arctic (63-90°N) stratospheric column ozone (1-100 hPa) vs. 2090s-mean surface N_2O for the four N_2O simulations (crosses), fitted with a simple linear regression model (black line). The grey shaded region indicates the 95% confidence interval for the slope and intercept of the regression model. (b-e) As for (a), but for: (b) the Antarctic (63-90°S); (c) northern midlatitudes (30-60°N); (d) southern midlatitudes (30-60°S); (e) the tropics (25°N-25°S).*

To test whether there is a quasi-linear relationship between stratospheric ozone at the end of the 21st century, and the N_2O or CH_4 concentration at that time, linear fits to 2090s-mean stratospheric ozone columns (1-100 hPa) as a function of N_2O or CH_4 concentrations were calculated in five regions of the stratosphere, as shown in Figures 5.6 and 5.7. The slopes for the linear fits in Figures 5.6 and 5.7 are given in Table 5.2, along with the R^2 values. To examine whether the linear fits are statistically significant, the 95% confidence intervals for the slopes and intercepts of the linear regression models were calculated, and are shown as the shaded regions in Figures 5.6 and 5.7.

As shown in Figure 5.6 and Table 5.2, the ozone-N_2O linear fits are statistically robust (the R^2 values exceed 0.94 everywhere) and the slopes are negative in all regions of the stratosphere. All slopes are significantly different from zero at the 95% confidence level, indicating a strong quasi-linear relationship between stratospheric ozone abundance and N_2O concentrations. The linear

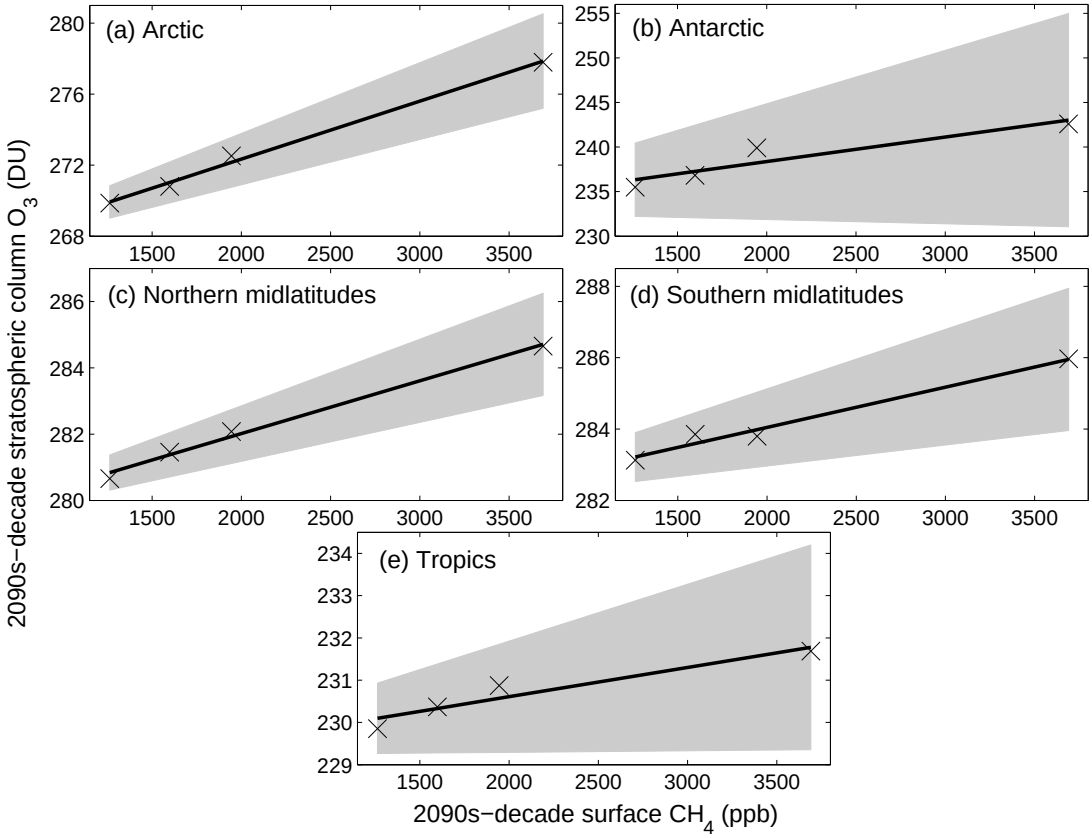

Figure 5.7: *Similar to Figure 5.6, but for 2090s-mean stratospheric column ozone vs. 2090s-mean surface CH_4 for the four CH_4 simulations.*

fits between ozone and CH_4 in Figure 5.7 are slightly poorer ($R^2 > 0.87$) but still statistically robust. All have positive slopes that are significantly different from zero at the 95% confidence level in all regions of the stratosphere except for the Antarctic, where the R^2 value is 0.87. For both the N_2O and CH_4 simulation data sets, sensitivities in the polar regions are enhanced (have steeper slopes) compared with those in the tropics and midlatitudes.

Figures 5.8 and 5.9 show the slopes of linear fits to 2090s-ozone vs. N_2O or CH_4 surface concentrations as a function of pressure and latitude. Regions where the slope is not statistically significantly different from zero at the 95% confidence bounds are hatched. Figure 5.8 shows that in the polar regions and throughout most of the middle stratosphere, ozone demonstrates a statistically significant negative linear relationship with N_2O. There is a weaker positive correlation in the tropical lower stratosphere, where enhanced N_2O leads to ozone production. Figure 5.9 shows that ozone decreases linearly with increasing CH_4 in the upper stratosphere, and that this relationship is statistically significant at the 95% confidence level. Statistically significant relationships between ozone and CH_4 are also found, for example, through much of the tropical, northern-midlatitude and Arctic stratosphere, where ozone increases with increasing CH_4.

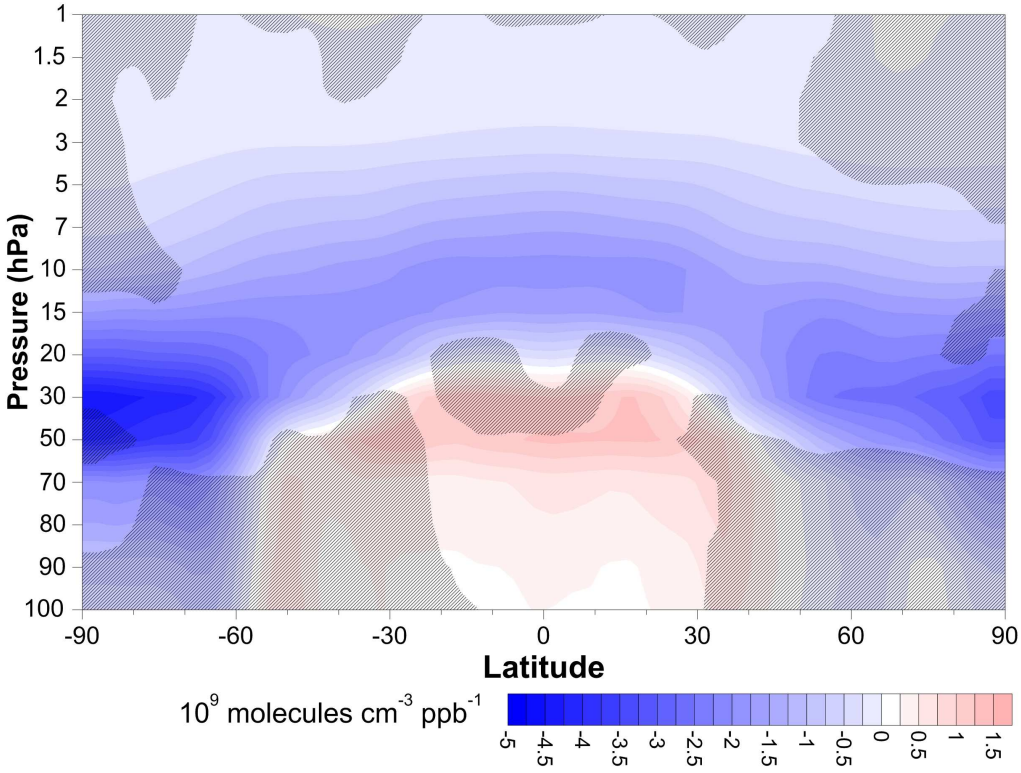

Figure 5.8: *Slopes from simple linear regression models fitted to 2090s-mean ozone vs. 2090s-mean surface N_2O for all latitudes and all pressure levels between 1-100 hPa, for the four N_2O simulations. Hatching indicates that the slope was not statistically significantly different from zero at the 95% level of confidence.*

Table 5.2: *Linear regression model fits of the data in Figures 5.6 and 5.7*

	N_2O simulations[a]		CH_4 simulations[b]	
	Slope[c]	R^2 value	Slope[c]	R^2 value
Arctic (63-90°N)	-10.4±7.8	0.942	7.9±1.7	0.995
Northern midlatitudes (30-60°N)	-7.1±1.3	0.996	3.9±1	0.993
Tropics (25°N-25°S)	-3±1	0.988	1.7±1.6	0.912
Southern midlatitudes (30-60°S)	-6.7±1.5	0.995	2.7±1.3	0.976
Antarctic (63-60°S)	-13.3±1.5	0.999	6.7±7.8	0.870

[a] *Data displayed in Figure 5.6.*
[b] *Data displayed in Figure 5.7.*
[c] *Slopes are units of DU ppb^{-1} and displayed alongside are the uncertainties on the slopes at the 95% confidence level.*

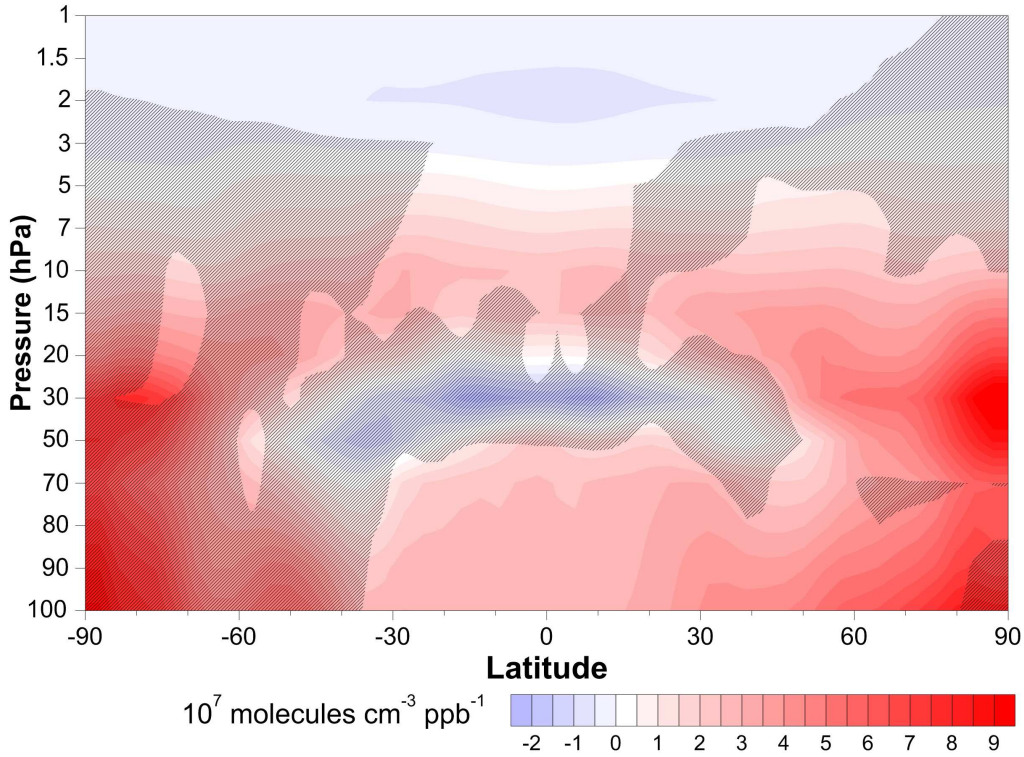

Figure 5.9: *Similar to Figure 5.8, but the slopes are from simple linear regression models fitted to 2090s-mean ozone vs. 2090s-mean surface CH_4 for the four CH_4 simulations.*

These linear relationships between ozone and N_2O and CH_4 over the range of RCP scenarios tested here suggest that perturbations to either stratospheric column ozone (using the results presented in Figures 5.6 and 5.7) or to vertically resolved ozone (using the results presented in Figures 5.8 and 5.9) can be incorporated into simple models of stratospheric ozone to capture the changes in ozone resulting from changes in N_2O and CH_4.

5.4 Conclusions

Total column ozone increases through the 21st century in all eight CCM simulations presented here. Larger increases are observed in simulations with low N_2O or high CH_4 concentrations. N_2O decreases stratospheric ozone abundance by increasing the rate of the ozone-depleting NO_x cycles. Although mid- and lower-stratospheric ozone increases in response to increased CH_4, upper-stratospheric ozone decreases due to an enhanced rate of the ozone-depleting HO_x cycles. Furthermore, it is shown here that at the end of the 21st century, stratospheric column ozone decreases linearly with increasing surface N_2O concentrations in all regions of the stratosphere. In contrast, stratospheric column ozone increases linearly with increasing CH_4 concentrations; however this relationship is not statistically significant at the 95% confidence level in the Antarc-

tic stratosphere. Vertically resolved relationships between ozone and N_2O, and ozone and CH_4 are presented here. The conclusions drawn from this work are derived from simulations based on a single CO_2 concentration scenario, and the apparent linear sensitivity of ozone under these conditions might not be sustained under different CO_2 scenarios.

Chapter 6

Summary, conclusions and outlook

The research undertaken for this thesis aimed to investigate the projected effects of anthropogenic GHG emissions on stratospheric ozone in the 21st century. To address this question, three CCM-based investigations were performed, and the results are presented in Chapters 3, 4 and 5.

The study described in Chapter 3 focusses on the effectiveness of N_2O in depleting stratospheric ozone in an evolving atmosphere over the period 1960-2100. The rates of a prescribed set of ozone-depleting cycles were tracked using the chemical cycle diagnostic implemented in the NIWA-SOCOL CCM (Section 2.3.2). Analysing the rates of the ozone-depleting NO_x cycles revealed the surprising result that ozone loss due to the primary NO_x cycle (Cycle I listed in Appendix A) is projected to decrease through the 21st century, despite N_2O concentrations increasing over that same period.

A number of factors act towards reducing NO_2 and O abundances, both of which are required in the rate-determining step of Cycle I. Processes leading towards decreased NO_2 abundances include:

- Projected strengthening of the Brewer-Dobson circulation through the 21st century due to warming SSTs, which increases the rate at which NO_y is removed from the stratosphere.
- Increasing concentrations of CO_2, which will continue to cool the stratosphere, thereby decreasing NO_y abundances through Reactions 3.2 and 3.3.
- Direct interactions between NO_x and other chemical families, for example with chlorine monoxide to produce $ClONO_2$, and with HO_x to produce HNO_3.

- Stratospheric cooling and decreases in chlorine loading through the 21st century, which are projected to decrease the NO_2/NO ratio.

Processes leading to decreased O abundances include:

- Competition for upper-stratospheric O from chlorine- and HO_x-catalysed ozone destruction cycles. Chlorine-induced ozone loss is expected to slow through the 21st century, following the phase-out of halocarbon emissions. HO_x-induced ozone loss is projected to speed up until mid-21st century and then begin to slow, following CH_4 concentrations (prescribed in the IPCC SRES A1B scenario).
- Stratospheric cooling decreases the O/O_3 ratio because Reaction 3.7 exhibits a large negative temperature-dependence.

Despite this list of factors projected to ameliorate the effect of N_2O on ozone, it is important to note that the conclusions drawn by *Randeniya et al.* [2002], *Ravishankara et al.* [2009], and later by *Portmann et al.* [2012], do not change: of all the ODSs currently emitted, N_2O remains the most important in the 21st century. However, the results presented in Chapter 3 highlight the importance of considering the entire radiative, chemical and dynamical environment of the stratosphere when assessing the effect of a single chemical species. As an example, increases in CH_4 lead to increases in reactive HO_x species, which slow Cycle I through a) competition for O from the HO_x ozone-loss cycles, and b) competition for NO_x by reacting to form HNO_3 (Reaction 3.5). This implies that the ozone-depletion potential (ODP) of N_2O is weakened by increases in CH_4. (An ODP for a chemical species quantifies the change in global ozone resulting from a unit emission of that species, relative to the change in global ozone resulting from an emission of the same unit mass of CFC-11 [*Daniel et al.*, 2011]). Given that the rate of the HO_x cycles maximises in the upper stratosphere (Figure 3.2(b)) where the ozone abundance is relatively small (Figure 1.1), this effect may be slight. Future work could focus on quantifying the degree to which the ODP of N_2O is lessened by CH_4.

Another conclusion derived from the study presented in Chapter 3 is that if N_2O emissions were to increase significantly, but CO_2 emissions were to undergo a relatively mild increase (or even a decrease, unlikely as it may seem in the current political climate), then this would lead to enhanced NO_x-induced ozone destruction. Not only would increased emissions of N_2O increase NO_x abundances, but a reduction in stratospheric cooling due to lower CO_2 abundances would also enhance NO_x-induced ozone loss. Such a scenario could occur if production and consumption of first-generation biofuels became widespread. Applications of nitrogen-based

fertilizers to crops would increase, so N_2O emissions would increase. At the same time, since biofuels are supposedly carbon-neutral, we could expect a reduction in fossil fuel burning and therefore in CO_2 emissions.

Exploring the effects of such a scenario on stratospheric ozone was the subject of the study presented in Chapter 4. Under a 'biofuels' GHG concentrations scenario, CCM results showed that global-mean column ozone decreases by 2.6 DU between 2010 and 2100. While this seems small, it must be placed in the context that global-mean ozone should theoretically *increase* through the 21st century (see, for example, Figure 2.2), as stratospheric halogen loading decreases due to the Montreal Protocol and as a result of stratospheric cooling. In summary, reducing CO_2 emissions while failing to limit N_2O emissions could be damaging to stratospheric ozone.

Substituting fossil fuels with biofuels to mitigate global climate change incurs many problems, aside from the ozone-depletion problem explored in Chapter 4. These include deforestation to obtain land suitable for agriculture, the large water volumes required to grow crops, and diverting crops from food to fuel. However, as noted by *Crutzen et al.* [2008], the environmental impacts of biofuels are crop-dependent. Calculations by *Davis et al.* [2012] showed that if the USA were to replace corn (which is used to produce ∼95% of the USA's biofuels) with switchgrass and miscanthus, then the central USA (where corn is predominantly grown) would transition from a net source to a net sink for GHGs.

While the studies presented in Chapters 3 and 4 explore the interactions between ozone and the GHGs CO_2, N_2O and CH_4 over time, the question addressed in Chapter 5 is "how sensitive is the ozone response to such GHG interactions?" Accordingly, CCM simulations were run in which the only input changed was the N_2O scenario *or* the CH_4 scenario. Changes in stratospheric chemistry resulting from increased concentrations of those GHGs lead to decreased stratospheric-column ozone in response to N_2O, and increased stratospheric-column ozone in response to CH_4. Ozone-GHG relationships in the Arctic, northern midlatitudes, tropics, southern midlatitudes and Antarctic were examined by fitting simple linear-regression models. The ozone-N_2O and ozone-CH_4 relationships are quasi-linear, and statistically significant (at the 95% confidence level) in all regions of the atmosphere, except for the ozone-CH_4 correlation in the Antarctic stratosphere. The implications of these results are that, for the SRES A1B CO_2 scenario at least, together with the SRES A1B CH_4 (or N_2O) scenario, the ozone response to N_2O (or CH_4) in the 21st century can be estimated without needing to run a CCM simulation. The results provide a simple parameterisation for use in SCMs. Future work should investigate the linearity

of the ozone response to N_2O and CH_4 under different CO_2 scenarios.

Throughout this thesis, it has been noted many times that increases in CO_2 and CH_4 are projected to lead to increases in global-mean stratospheric ozone. However, emissions of these gases should not be viewed as policy options for accelerating ozone recovery, due to their detrimental effects on the climate system as GHGs. Indeed, the Earth system is so highly interconnected that attempting to mitigate the effects of anthropogenic activities in one area of the Earth system inevitably has consequences for another. Such consequences may be advantageous, as in the case of the Antarctic ozone hole problem, whereby enacting the Montreal Protocol to phase out ODSs was beneficial in terms of reducing radiative forcing because the ozone-depleting halocarbons are also GHGs with large GWPs (Section 1.2.3). Consequences may also be injurious to some part of the Earth system; for example replacing fossil fuels with biofuels in an attempt to reduce CO_2 emissions, which may be damaging to the ozone layer.

Another possibility for reducing global radiative forcing which could have serious consequences for stratospheric ozone is sulfate geoengineering, which has not been discussed in this thesis. Sulfate geoengineering is a proposed practice of spraying sulfate aerosols into the stratosphere to reduce incoming solar radiation. Amongst numerous environmental and political issues, discussed for example by *Robock et al.* [2009], this could delay Antarctic ozone hole recovery and increase Arctic ozone depletion, due to cooling of the polar stratosphere and faster heterogeneous ozone loss reactions on sulfate aerosol particles [*Tilmes et al.*, 2008, 2009].

CCMs are continuing to undergo development to more accurately model the climate system and address issues such as how the climate system might be affected by geoengineering. Increasingly, modelling groups are moving towards coupling interactive oceans to their CCMs instead of using prescribed SSTs, since ocean feedbacks affect the relationship between ozone changes and lower tropospheric climate [*Morgenstern et al.*, 2010]. In addition, the importance of using coupled stratosphere-troposphere models for modelling atmospheric processes and for making projections of the future atmosphere has been recognized. For example, events in which dry and ozone-rich stratospheric air enters the troposphere alter tropospheric composition, and are particularly significant for cities that measure tropospheric ozone as an indicator of air pollution. Likewise, local air pollution has implications for the climate system as a whole. To this end, the next CCM validation activity (already underway), following on from CCMVal-2, aims to unite the stratospheric- and tropospheric-modelling communities.

The chemical cycle diagnostic used for the work presented in this thesis is currently implemented in only the NIWA-SOCOL CCM. While it could be implemented in other CCMs, other possibilities exist for extending its capabilities. One would be to couple it with a diagnostic such as that developed by *Garny et al.* [2011], which quantifies ozone changes due to transport and chemistry. This would enable detailed attribution of ozone changes. The chemical cycle diagnostic could also be extended to study tropospheric chemistry, which, alongside stratospheric chemistry, is currently undergoing rapid changes as a result of human activities.

The results presented in this thesis show that the GHGs CO_2, N_2O and CH_4 will play a large role in determining the evolution of stratospheric ozone through the 21st century, both in terms of their direct effects on ozone, and in terms of how the interactions between them subsequently affect ozone. However, the CCM projections presented here are based (and can only be based) on current scientific knowledge. Unprecedented changes in the composition of Earth's atmosphere and processes therein are likely to occur in the 21st century as a result of anthropogenic activities. In my view, understanding such changes and their subsequent impacts on the Earth system has never been of greater importance.

References

Atkins, P. W., *Physical Chemistry*. Oxford University Press, Oxford, UK, 6$^{\text{th}}$ edn., 1998.

Avallone, L. M., and M. J. Prather, Photochemical evolution of ozone in the lower tropical stratosphere, *Journal of Geophys. Res.*, *101*(D1), 1457–1461, 1996.

Baldwin, M., et al., *Climate-ozone connections, Chapter 5 in Scientific Assessment of Ozone Depletion: 2006*. Global Ozone Research and Monitoring Project, Report No. 50, 572 pp., World Meteorological Organization, Geneva, Switzerland, 2007.

Bates, D. R., and M. Nicolet, Atmospheric hydrogen, *Publ. Astron. Soc. Pac.*, *62*, 106–110, 1950.

Bekki, S., et al., *Future ozone and its impact on surface UV, Chapter 3 in Scientific Assessment of Ozone Depletion: 2010*. Global Ozone Research and Monitoring Project, Report No. 52, 516 pp., World Meteorological Organization, Geneva, Switzerland, 2011.

Bessou, C., F. Ferchaud, B. Gabrielle, and B. Mary, Biofuels, greenhouse gases and climate change. A review, *Agron. Sustain. Dev.*, *31*(1), 1–79, 2011.

Brasseur, G., and S. Solomon, *Aeronomy of the Middle Atmosphere*. Springer, Dordrecht, Netherlands, 3$^{\text{rd}}$ edn., 2005.

Brasseur, G. P., X. X. Tie, P. J. Rasch, and F. Lefèvre, A three-dimensional simulation of the Antarctic ozone hole: Impact of anthropogenic chlorine on the lower stratosphere and upper troposphere, *J. Geophys. Res.*, *102*(D7), 8909–8930, 1997.

Brasseur, G. P., R. G. Prinn, and A. A. P. Pszenny, *Atmospheric Chemistry in a Changing World*. Springer, Berlin, Germany, 2003.

Butchart, N., and A. A. Scaife, Removal of chlorofluorocarbons by increased mass exchange between the stratosphere and troposphere in a changing climate, *Nature*, *410*(6830), 799–802, 2001.

Butchart, N., et al., Chemistry-climate model simulations of twenty-first century stratospheric climate and circulation changes, *J. Climate*, *23*(20), 5349–5374, 2010.

Carslaw, K. S., B. Luo, and T. Peter, An analytic expression for the composition of aqueous HNO_3-H_2SO_4 stratospheric aerosols including gas-phase removal of HNO_3, *Geophys. Res. Lett.*, *22*(14), 1877–1880, 1995.

Chapman, S., On ozone and atomic oxygen in the upper atmosphere, *Philos. Mag.*, *10*(64), 369–383, 1930.

Chipperfield, M. P., and W. Feng, Comment on: Stratospheric ozone depletion at northern mid-latitudes in the 21st century: The importance of future concentrations of greenhouse gases nitrous oxide and methane, *Geophys. Res. Lett.*, *30*(7), 1389, 2003.

Cook, P. A., and H. K. Roscoe, Changes in reactive stratospheric gases due to a change in Brewer-Dobson circulation: results from a simple model, *Atmos. Sci. Lett.*, *13*(1), 49–54, 2012.

Crutzen, P. J., The influence of nitrogen oxides on the atmospheric ozone content, *Q. J. Roy. Meteor. Soc.*, *96*(408), 320–325, 1970.

Crutzen, P. J., Ozone production rates in an oxygen-hydrogen-nitrogen oxide atmosphere, *J. Geophys. Res.*, *76*(30), 7311–7327, 1971.

Crutzen, P. J., A. R. Mosier, K. A. Smith, and W. Winiwarter, N_2O release from agro-biofuel production negates global warming reduction by replacing fossil fuels, *Atmos. Chem. Phys.*, *8*(2), 389–395, 2008.

Damian, V., A. Sandu, M. Damian, F. Potra, and G. R. Carmichael, The kinetic preprocessor KPP - a software environment for solving chemical kinetics, *Comput. Chem. Eng.*, *26*, 1567–1579, 2002.

Daniel, J. S., G. J. M. Velders, A. R. Douglass, P. M. D. Forster, D. A. Hauglustaine, I. S. A. Isaksen, L. J. M. Kuijpers, A. McCulloch, and T. J. Wallington, *Halocarbon scenarios, ozone depletion potentials, and global warming potentials, Chapter 8 in Scientific Assessment of Ozone Depletion: 2006*. Global Ozone Research and Monitoring Project-Report No. 50, 572 pp., World Meterological Organization, Geneva, Switzerland, 2007.

Daniel, J. S., et al., *A focus on information and options for policymakers, Chapter 5 in Scientific Assessment of Ozone Depletion: 2010*. Global Ozone Research and Monitoring Project, Report No. 52, 516 pp., World Meteorological Organization, Geneva, Switzerland, 2011.

Davis, S. C., W. J. Parton, S. J. Del Grosso, C. Keough, E. Marx, P. R. Adler, and E. H. DeLucia, Impact of second-generation biofuel agriculture on greenhouse-gas emissions in the corn-growing regions of the US, *Front. Ecol. Environ.*, *10*(2), 69–74, 2012.

Denman, K. L., et al., *Couplings between changes in the climate system and biogeochemistry, Chapter 7 in Climate Change 2007: The Physical Science Basis. Contribution of Working Group I to the Fourth Assessment Report of the Intergovernmental Panel on Climate Change.* S. Solomon, D. Qin, M. Manning, Z. Chen, M. Marquis, K.B. Averyt, M.Tignor and H.L. Miller (Eds.), Cambridge University Press, Cambridge, UK, 2007.

Dessler, A., *The Chemistry and Physics of Stratospheric Ozone.* Academic Press, London, UK, 2000.

Douglass, A., et al., *Stratospheric ozone and surface ultraviolet radiation, Chapter 2 in Scientific Assessment of Ozone Depletion: 2010.* Global Ozone Research and Monitoring Project, Report No. 52, 516 pp., World Meteorological Organization, Geneva, Switzerland, 2011.

Egorova, T., E. Rozanov, V. Zubov, E. Manzini, W. Schmutz, and T. Peter, Chemistry-climate model SOCOL: A validation of the present-day climatology, *Atmos. Chem. Phys.*, *5*, 1557–1576, 2005.

Egorova, T. A., E. V. Rozanov, V. A. Zubov, and I. L. Karol, Model for investigating ozone trends (MEZON), *Izv. Russ. Acad. Sci. Atmos. Oceanic Phys. Engl. Transl.*, *39*(3), 277–292, 2003.

Eyring, V., et al., Multimodel projections of stratospheric ozone in the 21st century, *J. Geophys. Res.*, *112*(D16303), 2007.

Eyring, V., T. G. Shepherd, and D. W. Waugh, *(Eds.) SPARC Report on the Evaluation of Chemistry-Climate Models.* SPARC Rep. 5, WCRP-132, WMO/TD-No. 1526, 2010a.

Eyring, V., et al., Sensitivity of 21st century stratospheric ozone to greenhouse gas scenarios, *Geophys. Res. Lett.*, *37*(L16807), 2010b.

Farman, J. C., B. G. Gardiner, and J. D. Shanklin, Large losses of total ozone in Antarctica reveal seasonal ClO_x/NO_x interaction, *Nature*, *315*(6016), 207–210, 1985.

Fleming, E. L., C. H. Jackman, R. S. Stolarski, and A. R. Douglass, A model study of the impact of source gas changes on the stratosphere for 1850-2100, *Atmos. Chem. Phys.*, *11*(16), 8515–8541, 2011.

Fomichev, V. I., A. I. Jonsson, J. de Grandpré, S. R. Beagley, C. McLandress, K. Semeniuk, and T. G. Shepherd, Response of the middle atmosphere to CO_2 doubling: Results from the Canadian Middle Atmosphere Model, *J. Climate*, *20*(7), 1121–1144, 2007.

Forster, P., et al., *Changes in atmospheric constituents and in radiative forcing, Chapter 2 in Climate Change 2007: The Physical Science Basis. Contribution of Working Group I to the Fourth Assessment Report of the Intergovernmental Panel on Climate Change*. S. Solomon, D. Qin, M. Manning, Z. Chen, M. Marquis, K.B. Averyt, M.Tignor and H.L. Miller (Eds.), Cambridge University Press, Cambridge, UK, 2007.

Forster, P. M., et al., *Stratospheric changes and climate, Chapter 4 in Scientific Assessment of Ozone Depletion: 2010*. Global Ozone Research and Monitoring Project, Report No. 52, 516 pp., World Meteorological Organization, Geneva, Switzerland, 2011.

Garny, H., V. Grewe, M. Dameris, G. E. Bodeker, and A. Stenke, Attribution of ozone changes to dynamical and chemical processes in CCMs and CTMs, *Geosci. Model Dev.*, *4*(2), 271–286, 2011.

Holton, J. R., *An Introduction to Dynamic Meteorology*. Elsevier Academic Press, San Diego, California, USA, 4^{th} edn., 2004.

Hoppel, K., R. Bevilacqua, D. Allen, G. Nedoluha, and C. Randall, POAM III observations of the anomalous 2002 Antarctic ozone hole, *Geophys. Res. Lett.*, *30*(7), 2003.

Jacobson, M. Z., *Fundamentals of Atmospheric Modeling*. Cambridge University Press, Cambridge, UK, 2^{nd} edn., 2005.

Johnston, H., Reduction of stratospheric ozone by nitrogen oxide catalysts from supersonic transport exhaust, *Science*, *173*(3996), 517–522, 1971.

Jonsson, A. I., J. de Grandpré, V. I. Fomichev, J. C. McConnell, and S. R. Beagley, Doubled CO_2-induced cooling in the middle atmosphere: Photochemical analysis of the ozone radiative feedback, *J. Geophys. Res.*, *109*(D24103), 2004.

Kanzawa, H., and S. Kawaguchi, Large stratospheric sudden warming in Antarctic late winter and shallow ozone hole in 1988, *Geophys. Res. Lett.*, *17*, 77–80, 1990.

Krämer, M., et al., Intercomparison of stratospheric chemistry models under polar vortex conditions, *J. Atmos. Chem.*, *45*(1), 51–77, 2003.

Labitzke, K. G., and H. van Loon, *The Stratosphere*. Springer, Berlin, Germany, 1999.

Lanzendorf, E. J., T. F. Hanisco, P. O. Wennberg, R. C. Cohen, R. M. Stimpfle, J. G. Anderson, R. S. Gao, J. J. Margitan, and T. P. Bui, Establishing the dependence of $[HO_2]/[OH]$ on temperature, halogen loading, O_3, and NO_x based on in situ measurements from the NASA ER-2, *J. Phys. Chem. A*, *105*(9), 1535–1542, 2001.

Lee, A. M., R. L. Jones, I. Kilbane-Dawe, and J. A. Pyle, Diagnosing ozone loss in the extratropical lower stratosphere, *J. Geophys. Res.*, *107*(D11), 4110, 2002.

Madronich, S., and S. Flocke, *The role of solar radiation in atmospheric chemistry, in Handbook of Environmental Chemistry*. P. Boule (ed.), Springer-Verlag, Heidelberg, Germany, 1999.

Manabe, S., and R. T. Wetherald, The effects of doubling the CO_2 concentration on the climate of a general circulation model, *J. Atmos. Sci.*, *32*(1), 3–15, 1975.

Manney, G. L., et al., Unprecedented Arctic ozone loss in 2011, *Nature*, *478*(7370), 469–475, 2011.

Manning, M., and A. Reisinger, Broader perspectives for comparing different greenhouse gases, *Phil. Trans. Roy. Soc. A*, *369*, 1891–1905, 2011.

Manzini, E., N. A. McFarlane, and C. McLandress, Impact of the Doppler spread parameterization on the simulation of the middle atmosphere circulation using the MA/ECHAM4 general circulation model, *J. Geophys. Res.*, *102*(D22), 25751–25762, 1997.

McElroy, M. B., and J. C. McConnell, Nitrous oxide: A natural source of stratospheric NO, *J. Atmos. Sci.*, *28*, 1095–1098, 1971.

McElroy, M. B., R. J. Salawitch, S. C. Wofsy, and J. A. Logan, Reductions of Antarctic ozone due to synergistic interactions of chlorine and bromine, *Nature*, *321*, 759–762, 1986.

Meinshausen, M., S. C. B. Raper, and T. M. L. Wigley, Emulating coupled atmosphere-ocean and carbon cycle models with a simpler model, MAGICC6 – Part 1: Model description and calibration, *Atmos. Chem. Phys.*, *11*(4), 1417–1456, 2011a.

Meinshausen, M., T. M. L. Wigley, and S. C. B. Raper, Emulating coupled atmosphere-ocean and carbon cycle models with a simpler model, MAGICC6 – Part 2: Applications, *Atmos. Chem. Phys.*, *11*(4), 1457–1471, 2011b.

Melillo, J. M., et al., Indirect emissions from biofuels: How important?, *Science*, *326*(5958), 1397–1399, 2009.

Molina, L. T., and M. J. Molina, Production of Cl_2O_2 from the self-reaction of the ClO reaction, *J. Phys. Chem.*, *91*, 433–436, 1987.

Molina, M. J., and F. S. Rowland, Stratospheric sink for chlorofluoromethanes: chlorine atom-catalysed destruction of ozone, *Nature*, *249*(5460), 810–812, 1974.

Montzka, S. A., E. J. Dlugokencky, and J. H. Butler, Non-CO_2 greenhouse gases and climate change, *Nature*, *476*(7358), 43–50, 2011.

Morgenstern, O., et al., Review of the formulation of present-generation stratospheric chemistry-climate models and associated external forcings, *J. Geophys. Res.*, *115*(D00M02), 2010.

Nakicenovic, N., and R. E. Swart, *IPCC Special Report on Emissions Scenarios*. Cambridge University Press, Cambridge, UK, 2001.

Newman, P. A., et al., What would have happened to the ozone layer if chlorofluorocarbons (CFCs) had not been regulated?, *Atmos. Chem. Phys.*, *9*(6), 2113–2128, 2009.

Oman, L. D., D. W. Waugh, S. R. Kawa, R. S. Stolarski, A. R. Douglass, and P. A. Newman, Mechanisms and feedback causing changes in upper stratospheric ozone in the 21st century, *J. Geophys. Res.*, *115*(D05303), 2010.

Plummer, D. A., J. F. Scinocca, T. G. Shepherd, M. C. Reader, and A. I. Jonsson, Quantifying the contributions to stratospheric ozone changes from ozone depleting substances and greenhouse gases, *Atmos. Chem. Phys.*, *10*(18), 8803–8820, 2010.

Portmann, R. W., and S. Solomon, Indirect radiative forcing of the ozone layer during the 21st century, *Geophys. Res. Lett.*, *34*(L02813), 2007.

Portmann, R. W., J. S. Daniel, and A. R. Ravishankara, Stratospheric ozone depletion due to nitrous oxide: influences of other gases, *Phil. Trans. Roy. Soc. B*, *367*(1593), 1256–1264, 2012.

Randall, D. A., et al., *Climate models and their evaluation, Chapter 8 in Climate Change 2007: The Physical Science Basis. Contribution of Working Group I to the Fourth Assessment Report of the Intergovernmental Panel on Climate Change*. S. Solomon, D. Qin, M. Manning, Z. Chen, M. Marquis, K.B. Averyt, M.Tignor and H.L. Miller (Eds.), Cambridge University Press, Cambridge, UK, 2007.

Randeniya, L. K., P. F. Vohralik, and I. C. Plumb, Stratospheric ozone depletion at northern mid latitudes in the 21st century: The importance of future concentrations of greenhouse gases nitrous oxide and methane, *Geophys. Res. Lett.*, *29*(4), 2002.

Ravishankara, A. R., J. S. Daniel, and R. W. Portmann, Nitrous oxide (N_2O): The dominant ozone-depleting substance emitted in the 21st century, *Science*, *326*(5949), 123–125, 2009.

Revell, L. E., G. E. Bodeker, D. Smale, R. Lehmann, P. E. Huck, B. E. Williamson, E. Rozanov, and H. Struthers, The effectiveness of N_2O in depleting stratospheric ozone, *Geophys. Res. Lett.*, *39*(15806), 2012.

Robock, A., A. Marquardt, B. Kravitz, and G. Stenchikov, Benefits, risks, and costs of stratospheric geoengineering, *Geophys. Res. Lett.*, *36*, 2009.

Rosenfield, J. E., and A. R. Douglass, Doubled CO_2 effects on NO_y in a coupled 2D model, *Geophys. Res. Lett.*, *25*(23), 4381–4384, 1998.

Rosenfield, J. E., A. R. Douglass, and D. B. Considine, The impact of increasing carbon dioxide on ozone recovery, *J. Geophys. Res.*, *107*(D6), 4049, 2002.

Rowland, F. S., J. E. Spencer, and M. J. Molina, Stratospheric formation and photolysis of chlorine nitrate, *J. Phys. Chem.*, *80*, 2711–2713, 1976.

Rozanov, E. V., V. A. Zubov, M. E. Schlesinger, F. Yang, and N. G. Andronova, The UIUC three-dimensional stratospheric chemical transport model: Description and evaluation of the simulated source gases and ozone, *J. Geophys. Res.*, *104*(D9), 11755–11781, 1999.

Salawitch, R. J., et al., Chemical loss of ozone in the Arctic polar vortex in the winter of 1991-1992, *Science*, *261*(5125), 1146–1149, 1993.

Sander, S. P., et al., *Chemical Kinetics and Photochemical Data for Use in Atmospheric Studies.* Evaluation no. 15, JPL Publication 06-2, Jet Propulsion Laboratory, Pasadena, California, USA, 2006.

Sander, S. P., et al., *Chemical Kinetics and Photochemical Data for Use in Atmospheric Studies.* Evaluation no. 16, supplement to evaluation 15: Update of key reactions, JPL Publication 09-31, Jet Propulsion Laboratory, Pasadena, California, USA, 2009.

Schraner, M., et al., Technical note: Chemistry-climate model SOCOL: Version 2.0 with improved transport and chemistry/microphysics schemes, *Atmos. Chem. Phys.*, *8*(19), 5957–5974, 2008.

Seinfeld, J. H., and S. N. Pandis, *Atmospheric Chemistry and Physics: From Air Pollution to Climate Change.* John Wiley and Sons, Inc., Hoboken, New Jersey, USA, 2nd edn., 2006.

Smeets, E. M. W., L. F. Bouwman, E. Stehfest, D. P. van Vuuren, and A. Posthuma, Contribution of N_2O to the greenhouse gas balance of first-generation biofuels, *Glob. Change Biol.*, *15*(1), 1–23, 2009.

Solomon, S., R. R. Garcia, F. S. Rowland, and D. J. Wuebbles, On the depletion of Antarctic ozone, *Nature*, *321*, 755–758, 1986.

Solomon, S., R. W. Portmann, and D. W. J. Thompson, Contrasts between Antarctic and Arctic ozone depletion, *Proc. Nat. Acad. Sci.*, *104*(2), 445–449, 2007.

Staehelin, J., N. R. P. Harris, C. Appenzeller, and J. Eberhard, Ozone trends: A review, *Rev. Geophys.*, *39*(2), 231–290, 2001.

Stolarski, R. S., and R. J. Cicerone, Stratospheric chlorine: A possible sink for ozone, *Can. J. Chemistry*, *52*, 1610–1615, 1974.

Tilmes, S., R. Müller, and R. Salawitch, The sensitivity of polar ozone depletion to proposed geoengineering schemes, *Science*, *320*(5880), 1201–1204, 2008.

Tilmes, S., R. R. Garcia, D. E. Kinnison, A. Gettelman, and P. J. Rasch, Impact of geoengineered aerosols on the troposphere and stratosphere, *J. Geophys. Res.*, *114*(D12305), 2009.

van Vuuren, D. P., et al., The representative concentration pathways: An overview, *Climatic Change*, *109*(1-2), 5–31, 2011.

Velders, G. J. M., S. O. Andersen, J. S. Daniel, D. W. Fahey, and M. McFarland, The importance of the Montreal Protocol in protecting climate, *P. Natl. Acad. Sci. USA*, *104*(12), 4814–4819, 2007.

West, J. J., S. Szopa, and D. A. Hauglustaine, Human mortality effects of future concentrations of tropospheric ozone, *Comptes Rendus Geoscience*, *339*(1112), 775–783, 2007.

WMO, *World Meteorological Organisation Scientific Assessment of Ozone Depletion: 2010.* Global Ozone Research and Monitoring Project, Report No. 52, 516 pp., Geneva, Switzerland, 2010.

Wofsy, S. C., M. B. McElroy, and Y. L. Yung, The chemistry of atmospheric bromine, *Geophys. Res. Lett.*, *2*, 215–218, 1975.

Wohltmann, I., R. Lehmann, and M. Rex, The Lagrangian chemistry and transport model ATLAS: simulation and validation of stratospheric chemistry and ozone loss in the winter 1999/2000, *Geosci. Model Dev.*, *3*(2), 585–601, 2010.

Wuebbles, D. J., and K. Hayhoe, Atmospheric methane and global change, *Earth-Sci. Rev.*, *57*(3-4), 177–210, 2002.

Zubov, V. A., E. V. Rozanov, and M. E. Schlesinger, Hybrid scheme for three-dimensional advective transport, *Mon. Weather Rev.*, *127*(6), 1335–1346, 1999.

Appendix A
Catalytic cycles tracked in NIWA-SOCOL

Rate-determining steps in bold.

Cycle I:

$$\mathrm{NO} + \mathrm{O_3} \longrightarrow \mathrm{NO_2} + \mathrm{O_2}$$

$$\underline{\mathbf{NO_2 + O \longrightarrow NO + O_2}}$$

$$\mathrm{O_3} + \mathrm{O} \longrightarrow 2\mathrm{O_2}$$

Cycle II:

$$\mathrm{NO} + \mathrm{O_3} \longrightarrow \mathrm{NO_2} + \mathrm{O_2}$$

$$\mathrm{NO_2} + \mathrm{O_3} \longrightarrow \mathrm{NO_3} + \mathrm{O_2}$$

$$\underline{\mathbf{NO_3} + \mathrm{h}\nu \longrightarrow \mathbf{NO} + \mathbf{O_2}}$$

$$2\mathrm{O_3} \longrightarrow 3\mathrm{O_2}$$

Cycle IIIa:

$$2(\mathrm{O_3} + \mathrm{h}\nu \longrightarrow \mathrm{O_2} + \mathrm{O}(^1\mathrm{D}))$$

$$\mathrm{O}(^1\mathrm{D}) + \mathrm{N_2} + \mathrm{M} \longrightarrow \mathrm{N_2O} + \mathrm{M}$$

$$\underline{\mathbf{O}(^\mathbf{1}\mathbf{D}) + \mathbf{N_2O} \longrightarrow \mathbf{N_2} + \mathbf{O_2}}$$

$$2\mathrm{O_3} \longrightarrow 3\mathrm{O_2}$$

Cycle IIIb:

$$2(O_3 + h\nu \longrightarrow O_2 + O(^1D))$$

$$O(^1D) + N_2 + M \longrightarrow N_2O + M$$

$$\underline{\mathbf{O(^1D) + N_2O \longrightarrow 2NO}}$$

$$2O_3 + N_2 \longrightarrow 2O_2 + 2NO$$

Cycle IV:

$$\mathbf{HO_2 + O_3 \longrightarrow OH + 2O_2}$$

$$\underline{OH + O_3 \longrightarrow HO_2 + O_2}$$

$$2O_3 \longrightarrow 3O_2$$

Cycle V:

$$\mathbf{HO_2 + O \longrightarrow OH + O_2}$$

$$\underline{OH + O_3 \longrightarrow HO_2 + O_2}$$

$$O_3 + O \longrightarrow 2O_2$$

Cycle VI:

$$OH + O \longrightarrow H + O_2$$

$$\underline{\mathbf{H + O_3 \longrightarrow OH + O_2}}$$

$$O_3 + O \longrightarrow 2O_2$$

Cycle VIIa:

$$O_3 + h\nu \longrightarrow O_2 + O(^1D)$$

$$O(^1D) + H_2O \longrightarrow 2OH$$

$$OH + O_3 \longrightarrow HO_2 + O_2$$

$$OH + H_2O_2 \longrightarrow H_2O + HO_2$$

$$\underline{\mathbf{HO_2 + HO_2 \longrightarrow H_2O_2 + O_2}}$$

$$2O_3 \longrightarrow 3O_2$$

Cycle VIIb:

$$H_2O_2 + h\nu \longrightarrow 2OH$$

$$2(OH + O_3 \longrightarrow HO_2 + O_2)$$

$$\underline{\mathbf{HO_2 + HO_2 \longrightarrow H_2O_2 + O_2}}$$

$$2O_3 \longrightarrow 3O_2$$

Cycle VIII:

$$O_3 + h\nu \longrightarrow O_2 + O(^1D)$$

$$O(^1D) + H_2O \longrightarrow 2OH$$

$$OH + O_3 \longrightarrow HO_2 + O_2$$

$$\underline{\mathbf{OH + HO_2 \longrightarrow H_2O + O_2}}$$

$$2O_3 \longrightarrow 3O_2$$

Cycle IX:

$$Cl + O_3 \longrightarrow ClO + O_2$$

$$\underline{\mathbf{ClO + O \longrightarrow Cl + O_2}}$$

$$O_3 + O \longrightarrow 2O_2$$

Cycle X:

$$O_3 + h\nu \longrightarrow O_2 + O(^1D)$$

$$O(^1D) + H_2O \longrightarrow 2OH$$

$$OH + O_3 \longrightarrow HO_2 + O_2$$

$$\mathbf{Cl + HO_2 \longrightarrow HCl + O_2}$$

$$\underline{OH + HCl \longrightarrow H_2O + Cl}$$

$$2O_3 \longrightarrow 3O_2$$

Cycle XI:

$$\mathrm{ClO + ClO + M \longrightarrow Cl_2O_2 + M}$$

$$\mathbf{Cl_2O_2 + h\nu \longrightarrow ClO_2 + Cl}$$

$$\mathrm{ClO_2 + M \longrightarrow Cl + O_2 + M}$$

$$\underline{\mathrm{2(Cl + O_3 \longrightarrow ClO + O_2)}}$$

$$\mathrm{2O_3 \longrightarrow 3O_2}$$

Cycle XII:

$$\mathrm{ClO + NO_2 + M \longrightarrow ClONO_2 + M}$$

$$\mathbf{ClONO_2 + O \longrightarrow ClO + NO + O_2}$$

$$\underline{\mathrm{NO + O_3 \longrightarrow NO_2 + O_2}}$$

$$\mathrm{O_3 + O \longrightarrow 2O_2}$$

Cycle XIII:

$$\mathbf{ClO + HO_2 \longrightarrow HOCl + O_2}$$

$$\mathrm{HOCl + h\nu \longrightarrow OH + Cl}$$

$$\mathrm{Cl + O_3 \longrightarrow ClO + O_2}$$

$$\underline{\mathrm{OH + O_3 \longrightarrow HO_2 + O_2}}$$

$$\mathrm{2O_3 \longrightarrow 3O_2}$$

Cycle XIV:

$$\mathbf{BrO + HO_2 \longrightarrow HOBr + O_2}$$

$$\mathrm{HOBr + h\nu \longrightarrow OH + Br}$$

$$\mathrm{Br + O_3 \longrightarrow BrO + O_2}$$

$$\underline{\mathrm{OH + O_3 \longrightarrow HO_2 + O_2}}$$

$$\mathrm{2O_3 \longrightarrow 3O_2}$$

Cycle XVa:

$$\mathbf{BrO + ClO \longrightarrow Br + ClO_2}$$

$$ClO_2 + M \longrightarrow Cl + O_2 + M$$

$$Br + O_3 \longrightarrow BrO + O_2$$

$$\underline{Cl + O_3 \longrightarrow ClO + O_2}$$

$$2O_3 \longrightarrow 3O_2$$

Cycle XVb:

$$\mathbf{BrO + ClO \longrightarrow BrCl + O_2}$$

$$BrCl + h\nu \longrightarrow Br + Cl$$

$$Br + O_3 \longrightarrow BrO + O_2$$

$$\underline{Cl + O_3 \longrightarrow ClO + O_2}$$

$$2O_3 \longrightarrow 3O_2$$

Cycle XVI:

$$O_2 + h\nu \longrightarrow O + O$$

$$O + O_2 + M \longrightarrow O_3 + M$$

$$O_3 + h\nu \longrightarrow O_2 + O$$

$$\underline{\mathbf{O + O_3 \longrightarrow 2O_2}}$$

$$O_3 \longrightarrow O + O_2$$